Reversible Carbon Monoxide Reactions of Cationic Rh(I) and Rh(II) Complexes

Steven C. Haefner,[†] Kim R. Dunbar,*[,†,§] and Christopher Bender[‡]

Contribution from the Department of Chemistry, Michigan State University, East Lansing, Michigan 48824. *Received June 5, 1991*

Abstract: The syntheses, spectral properties, redox chemistry, and structures of complexes obtained from the reaction of carbon monoxide with a rare mononuclear Rh(II) species are described. The ionic compound $[Rh(\eta^3\text{-TMPP})_2][BF_4]_2$ (**1**) {TMPP = tris(2,4,6-trimethoxyphenyl)phosphine, $P(C_6H_2(OMe)_3)_3$} has been prepared in high yield by reaction of the unbridged Rh_2^{4+} complex $[Rh_2(CH_3CN)_{10}][BF_4]_4$ with 4 equiv of TMPP in CH_3CN. The product crystallizes in the orthorhombic space group *Pbcn* with unit cell dimensions a = 15.938 (5) Å, b = 17.916 (7) Å, c = 21.015 (8) Å, V = 5376 (3) Å^3, and Z = 4. Residuals of R = 0.073 and R_w = 0.089 were obtained after least-squares refinement of 369 parameters to convergence and a quality-of-fit of 2.37. The Rh atom, which is situated on a 2-fold axis, is bonded to two ether phosphine groups in a capping, tridentate mode through the phosphorus atom and two *o*-methoxy substituents. The geometry about the metal is pseudooctahedral, and, surprisingly, the phosphorus atoms lie cis to one another. A Jahn-Teller structural distortion was observed for **1** along the direction of the two trans oxygen atoms, which constitutes the first documentation of this effect in a molecular Rh(II) d^7 complex. $[Rh(\eta^3\text{-TMPP})_2][BF_4]_2$ was also characterized by infrared, electronic and EPR spectroscopies, and by elemental analysis. Complex **1** reacts reversibly with carbon monoxide by a series of redox reactions, initiated by a highly unstable Rh(II) dicarbonyl adduct. Products isolated from the reaction under a CO atmosphere are the Rh(III) complex $[Rh(\eta^3\text{-TMPP})_2][BF_4]_3$ (**2**) and the Rh(I) dicarbonyl complex $[Rh(TMPP)_2(CO)_2][BF_4]$ (**3**). Compound **3** has been crystallized as its CH_2Cl_2 solvate in the space group $P\bar{1}$ with unit cell dimensions a = 13.318 (4) Å, b = 13.404 (2) Å, c = 18.104 (4) Å, α = 95.908 (3)°, β = 97.037 (3)°, γ = 90.711 (3)°, V = 3200 (2) Å^3, and Z = 2. Least-squares refinement of 779 parameters gave residuals of R = 0.059 and R_w = 0.084 and a quality-of-fit = 2.316. The Rh(I) cation occupies a general position and exhibits a trans square-planar coordination geometry, with the phosphine ligands acting as monodentate groups. In the absence of a CO atmosphere, **3** readily loses a molecule of CO to form the monocarbonyl species $[Rh(\eta^2\text{-TMPP})(TMPP)CO][BF_4]$ (**4**) which has been structurally characterized as the benzene solvate $[Rh(\eta^2\text{-TMPP})(TMPP)CO][BF_4]\cdot 2C_6H_6$: triclinic space group $P\bar{1}$ with unit cell dimensions of a = 14.898 (5) Å, b = 18.060 (8) Å, c = 14.343 (4) Å, α = 96.56 (4)°, β = 113.84 (2)°, γ = 104.80 (4)°, V = 3308 (2) Å^3, and Z = 2. Final refinement of 757 parameters gave residuals of R = 0.067 and R_w = 0.069 with a quality-of-fit of 2.59. The immediate coordination sphere of the Rh atom consists of one CO ligand and two trans phosphorus atoms with the fourth site being occupied by a pendant methoxy group. The resulting structure is a highly distorted square-planar arrangement as evidenced by the bond angle O(1)-Rh(1)-C(55) of 150.2 (4)°. Complex **4** reversibly adds CO, both in the solid state and in solution, to reform **3**. Furthermore, $[Rh(\eta^2\text{-TMPP})(TMPP)CO]^{1+}$ (**4**) undergoes a second electron-transfer process with $[Rh(\eta^3\text{-TMPP})_2][BF_4]_3$ (**2**) to form $[Rh(\eta^3\text{-TMPP})_2]^{2+}$ (**1**) and the unstable Rh(II) complex $[Rh(TMPP)_2(CO)]^{2+}$. The latter can easily lose CO to regenerate the original Rh(II) radical species **1** or add a second CO, thereby continuing the cycle. The quantitative regeneration of the parent Rh(II) complex is ultimately limited by the thermal instability of $[Rh(\eta^3\text{-TMPP})_2]^{3+}$, which undergoes a demethylation reaction at room temperature to give the Rh(III) species $[Rh(\eta^3\text{-TMPP})(P\{C_6H_2(OMe)_2O\}\{C_6H_2(OMe)_3\}_2)][BF_4]_2$ (**5**) with a phenoxide interaction. Compound **5** has been fully characterized by NMR, electrochemistry, and elemental analysis. Complexes **2-5** have also been prepared in high yield by separate routes and independently characterized.

Introduction

Recent synthetic strategies in our group have allowed for the high-yield preparation of divalent mononuclear rhodium complexes. These systems all have in common the presence of an unusual phosphine with the combined characteristics of high basicity, large size, and functionality. The ligand, tris(2,4,6-trimethoxyphenyl)phosphine (TMPP), which was reported as long ago as 1959 by Soviet chemists,[1] has not been widely used in transition-metal chemistry despite its ease of preparation, stability, and inherently desirable properties for stabilizing unusual reaction centers. In fact, we know of only two reports of complexes containing the TMPP ligand; these are $[M(TMPP)_2]^+$ (M = Cu, Ag) and CuX(TMPP) (X = Cl, Br).[3] Organic chemists, Wada and co-workers, reintroduced the ligand to the recent literature, with reports of mild ring-opening reactions of terminal epoxides[3] and extraordinarily facile dealkylation reactions, findings that could lead to applications in catalytic polymerization of olefins and in Michael additions.[4] Clearly, the extreme nucleophilicity of the phosphorus lone pair imparts unusual reactivity to this tertiary phosphine.

Apart from its organic applications, TMPP shows promise in coordination and organometallic chemistry due to the presence of methoxy substituents that are capable of binding weakly to a metal. One can easily envision at least three coordination modes for the neutral ligand ranging from monodentate (η^1) to tridentate (η^3) as in **a-c** below and two bonding arrangements for the anionic phenoxide derivative **d** and **e**. Crystallographic evidence for coordination of a pendant ether group was first provided by Graziani and co-workers with the structure of the Rh(III) arsine complex, $RhCl_3[(AsMe_2(o\text{-}C_6H_4(OMe)]_2$.[5] Later in the mid-1970s, Shaw and, independently, Roundhill and Rauchfuss reported that 2-methoxyphenylphosphines coordinate to metals such as Ir, Pt, and Ru through interactions of the oxygen atom in the ortho position of the phenyl ring.[6] These complexes with very weak and,

[†] Michigan State University.
[‡] Albert Einstein College of Medicine of Yeshiva University.
[§] Camille and Henry Dreyfus Teacher-Scholar 1991-1995.

(1) (a) Protopopov, I. S.; Kraft, M. Y. *Zhurnal Obshchei Khimii* **1963**, *33*, 3050. (b) Protopopov, I. S.; Kraft, M. Y. *Med. Prom. SSSR* **1959**, *13*, 5; *Chem. Abstr.* **1960**, *54*, 10914c.

(2) (a) Wada, M.; Higashizaki, S. *J. Chem. Soc., Chem. Commun.* **1984**, 482. (b) Wada, M.; Higashizaki, S.; Tsuboi, A. *J. Chem. Res.* **1985**, (S), 38; (M), 0467. (c) Bowmaker, G. A.; Cotton, J. D.; Healy, P. C.; Kildea, J. D.; Silong, S. B.; Skelton, B. W.; White, A. H. *Inorg. Chem.* **1989**, *28*, 1462.

(3) Wada, M.; Tsuboi, A. *J. Chem. Soc., Perkin Trans. I* **1987**, 151.

(4) Wada, M.; Tsuboi, A.; Nishimura, K.; Erabi, T. *Nippon Kagaku Kaishi* **1987**, *7*, 1284.

(5) Graziani, R.; Bombiere, G.; Volponi, L.; Panattoni, C.; Clark, R. J. H. *J. Chem. Soc. (A)* **1969**, 1236.

(6) (a) Mason, R.; Thomas, K. M.; Empasall, H. D.; Fletcher, S. R.; Heys, P. N.; Hyde, E. M.; Jones, C. E.; Shaw, B. L. *J. Chem. Soc., Chem. Commun.* **1974**, 612. (b) Jones, C. E.; Shaw, B. L.; Turtle, B. L. *J. Chem. Soc., Dalton Trans.* **1974**, 993. (c) Rauchfuss, T. B.; Patino, F. T.; Roundhill, D. M. *Inorg. Chem.* **1975**, *14*, 652. (d) Jeffrey, J. C.; Rauchfuss, T. B. *Inorg. Chem.* **1979**, *18*, 2658.

0002-7863/91/1513-9540$02.50/0

therefore, labile, metal–ether interactions have been referred to as "incipiently" coordinatively unsaturated molecules with hemilabile ligands.[6d,7,8]

TMPP (neutral)

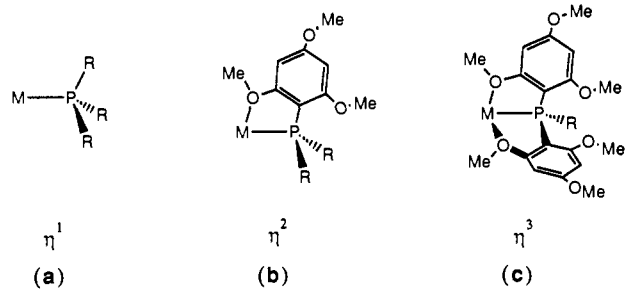

η^1 (a) η^2 (b) η^3 (c)

TMPP-*O* (anionic)

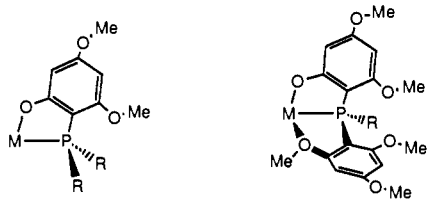

η^2 (d) η^3 (e)

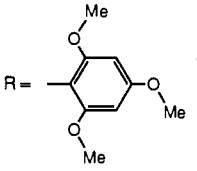

It is important in the context of the present work to note that the aforementioned chemistry of ether phosphines did not address the effects of bulk and high phosphorus basicity on the reactivity of the ligand. A functionalized phosphine with these characteristics opens up the possibility of designing metal complexes with unusual oxidation states, even odd-electron species, due to the combined kinetic and chelate stabilization effects. Moreover the highly donating (soft) nature of the phosphorus atom serves to counterbalance the relative incompatibility of the harder ether ligands with softer, low-valent metal centers. Metal complexes that form interactions with both donor types undergo facile substitution reactions as an ether group labilizes in favor of an incoming substrate, but since the displaced group does not leave the metal complex, the starting material regenerates upon completion of the reaction.[9]

We have discovered that an excellent area of application for the TMPP ligand is the stabilization of mononuclear Rh(II) complexes. Conventional wisdom is that isolated d^7 rhodium centers, unlike their Co(II) analogues, are unstable due to their proclivity for forming M–M bonds, but paramagnetic Rh(II) compounds have in fact been documented.[10] For example, it has been known for years that $RhCl_3$ reacts with various sterically encumbering phosphines to produce compounds of general formula $RhX_2(PR_3)_2$ (X = Cl, Br).[11] Unfortunately, problems with decomposition and a general lack of structural data have slowed the progress of this area of coordination chemistry, but recent reports of crown thioether and other sulfur complexes of Rh(II) have contributed to the growing body of literature on the synthesis of mononuclear Rh(II) compounds.[12] The reactivity of these rare species has been relatively unexplored, however, with only a few studies having appeared.[13]

Our own research in mononuclear Rh(II) phosphine chemistry, using the solvated binuclear complex $[Rh_2(CH_3CN)_{10}]^{4+}$ as a starting material, has resulted in the first example of a structurally characterized six-coordinate Rh(II) complex without a metal–metal bond; the cation, $[Rh(\eta^3\text{-TMPP})_2]^{2+}$, exhibits EPR, magnetic properties, and the anticipated Jahn–Teller distortion for a d^7 metal configuration in a dz^2 ground state. Reactions of this highly unusual cation with small molecules are quite interesting, allowing access to new stable paramagnetic Rh(II) complexes in addition to disproportionation products. Herein we report the reversible chemistry of $[Rh(\eta^3\text{-TMPP})_2][BF_4]_2$ with carbon monoxide which cycles through a series of redox reactions. We also report the reversible and selective reactivity of a Rh(I) complex with CO in solution and in the solid state. Some of these results have appeared in communication form.[14]

Experimental Section

Starting Materials. The solvated dirhodium complex, $[Rh_2(CH_3CN)_{10}][BF_4]_4$, was prepared as described in the literature.[15] The starting material $[Rh(cod)Cl]_2$ was purchased from Strem Chemicals. Tris(2,4,6-trimethoxyphenyl)phosphine (TMPP) was prepared by the reaction of triphenylphosphite with the lithium salt of 1,3,5-trimethoxybenzene.[16] Carbon monoxide was obtained from Matheson Gas Products and was used as received. $[Cp_2Fe][BF_4]$ was prepared by oxidation of Cp_2Fe with hydrofluoroboric acid in the presence of *p*-benzoquinone.[17] The reagents $NOBF_4$, $NOPF_6$, and Cp_2Co were purchased from Strem Chemicals and used without further purification. The gas ^{13}CO (99%) was purchased from Aldrich. All solvents were predried over 4Å molecular sieves. Benzene, toluene, diethyl ether, and THF were distilled from sodium/potassium benzophenone ketyl radical, whereas methylene chloride, acetonitrile, and methanol were distilled under a nitrogen atmosphere from P_2O_5, CaH_2, and $Mg(OCH_3)_2$, respectively.

Reaction Procedures. All reactions were carried out under an argon atmosphere by the use of standard Schlenk-line techniques unless otherwise stated. Reactions at pressures greater than 1 atm were performed in a 450-mL stainless steel Parr mini reactor (Model 4560) equipped with a magnetic drive stirrer and an automatic temperature control.

Preparation of $[Rh(\eta^3\text{-TMPP})_2][BF_4]_2$ (1). An amount of $[Rh_2(CH_3CN)_{10}][BF_4]_4$ (0.300 g, 0.311 mmol) was dissolved in 3 mL of CH_3CN, and 4 equiv of TMPP (0.603 g, 1.24 mmol) in 15 mL of CH_3CN were added dropwise at 0 °C over the period of 30 min. The resulting

(7) (a) Alcock, N. W.; Brown, J. M.; Jeffery, J. C. *J. Chem. Soc., Dalton Trans.* **1976**, 583. (b) Anderson, G. K.; Kumar, R. *Inorg. Chem.* **1984**, *23*, 4064. (c) Anderson, G. K.; Corey, E. R.; Kumar, R. *Inorg. Chem.* **1987**, *26*, 97. (d) Anderson, G. K.; Kumar, R. *Inorg. Chim. Acta* **1988**, *146*, 89. (e) Alcock, N. W.; Platt, A. W. G.; Pringle, P. G. *J. Chem. Soc., Dalton Trans.* **1989**, 2069. (f) Reddy, V. V. S.; Whitten, J. E.; Redmill, K. A.; Varshney, A.; Gray, G. M. *J. Organomet. Chem.* **1989**, *372*, 207. (g) Reddy, V. V. S.; Varshney, A.; Gray, G. M. *J. Organomet. Chem.* **1990**, *391*, 259.

(8) Bader, A.; Lindner, E. *Coord. Chem. Rev.* **1991**, *108*, 27 and references therein.

(9) (a) Rauchfuss, T. B. *Homogeneous Catalysis with Metal Phosphine Complexes*; Pignolet, L., Ed.; Plenum, New York, 1983; p 239.

(10) (a) Felthouse, T. R. *Prog. Inorg. Chem.* **1982**, *29*, 73. (b) Cotton, F. A.; Walton, R. A. *Multiple Bonds between Metal Atoms*; John Wiley and Sons, New York, 1982. (c) Billig, E.; Shupack, S. I.; Waters, J. H.; Williams, R.; Gray, H. B. *J. Am. Chem. Soc.* **1964**, *86*, 926.

(11) (a) Bennett, M. A.; Lonstaff, P. A. *J. Am. Chem. Soc.* **1969**, *91*, 6266. (b) Moers, F. G.; DeJong, J. A. M.; Beaumont, P. M. J. *J. Inorg. Nucl. Chem.* **1973**, *36*, 1915. (c) Masters, C.; Shaw, B. L. *J. Chem. Soc. (A)* **1971**, 3679. (d) Empsall, H. D.; Heys, P. N.; Shaw, B. L. *Transition Met. Chem.* **1978**, *3*, 165. (e) Empsall, H. D.; Hyde, E. M.; Pawson, D.; Shaw, B. L. *J. Chem. Soc., Dalton Trans.* **1977**, 1292.

(12) (a) Rawle, S. C.; Yagbasan, R.; Prout, K.; Cooper, S. R. *J. Am. Chem. Soc.* **1987**, *109*, 6181. (b) Blake, A. J.; Gould, R. D.; Holder, A. J.; Hyde, T. I.; Schröder, M. *J. Chem. Soc., Dalton Trans.* **1988**, 1861. (c) Cooper, S. R.; Rawle, S. C.; Yagbasan, R.; Watkin, D. J. *J. Am. Chem. Soc.* **1991**, *113*, 1600. (d) Pneumatikakis, G.; Psaroulis, P. *Inorg. Chim. Acta* **1980**, *46*, 97. (e) Pandey, K. K.; Nehete, D. T.; Sharma, R. B. *Polyhedron* **1990**, *9*, 2013.

(13) (a) Vleck, A. *Inorg. Chim. Acta* **1980**, *43*, 35. (b) Holah, D. G.; Hughes, A. N.; Hui, B. C. *Can. J. Chem.* **1975**, *53*, 3669. (c) Valentini, G.; Braca, G.; Sbrana, G.; Colligiani, A. *Inorg. Chim. Acta* **1983**, *69*, 215. (d) Valentini, G.; Braca, G.; Sbrana, G.; Colligiani, A. *Inorg. Chim. Acta* **1983**, *69*, 221.

(14) (a) Dunbar, K. R.; Haefner, S. C.; Pence, L. E. *J. Am. Chem. Soc.* **1989**, *111*, 5504. (b) Dunbar, K. R.; Haefner, S. C.; Swepston, P. N. *J. Chem. Soc., Chem. Commun.* **1991**, 460.

(15) (a) Dunbar, K. R. *J. Am. Chem. Soc.* **1988**, *110*, 8247. (b) Dunbar, K. R.; Pence, L. E. *Inorg. Synth.* **1991**, *29*, in press.

(16) (a) Wada, M.; Higashizaki, S. J. *J. Chem. Soc., Chem. Commun.* **1984**, 482. (b) Dunbar, K. R.; Haefner, S. C., manuscript in preparation.

(17) Gray, H. B.; Hendrickson, D. N.; Sohn, Y. S. *Inorg. Chem.* **1971**, *10*, 1559.

deep purple solution was stirred for an additional 15 min and evaporated to a residue with a rotary evaporator. The crude solid was washed with copius amounts of THF, dissolved in 40 mL of CH_2Cl_2, and filtered. THF (10 mL) was added, and the volume was reduced to approximately 10–15 mL to produce a purple crystalline sample which was collected by filtration, washed with 3 × 10 mL of THF, and dried under reduced pressure: yield 0.80 g (82%). Anal. Calcd for $C_{55}H_{66}F_8P_2O_{18}B_2Rh$: C, 48.34; H, 4.96. Found: C, 48.56; H, 4.86.

Preparation of $[Rh(\eta^3\text{-TMPP})_2][BF_4]_3$ (2). (i) Oxidation of $[Rh(\eta^3\text{-TMPP})_2][BF_4]_2$ with $NOBF_4$. A quantity of $[Rh(\eta^3\text{-TMPP})_2][BF_4]_2$ (0.200 g, 0.14 mmol) and $NOBF_4$ (0.016 g, 0.14 mmol) was dissolved in 5 mL of acetonitrile, resulting in the immediate formation of a deep red solution. The reaction was stirred at −40 °C for 45 min with periodic pumping to remove the evolved NO gas, after which time 20 mL of diethyl ether was added to precipitate the product. The red solid was collected by filtration under argon, washed with 3 × 5 mL of diethyl ether, and dried in vacuo: yield, 0.085 g (80%). Anal. Calcd for $C_{54}H_{66}F_{12}P_2O_{18}B_3Rh$: C, 45.40; H, 4.66. Found: C, 44.39; H, 5.14. Due to thermal instability, solid and solution forms of **2** must be stored anaerobically at −20 °C.

(ii) Oxidation of $[Rh(\eta^3\text{-TMPP})_2][BF_4]_2$ with $[Cp_2Fe][BF_4]$. A solution of $[Rh(\eta^3\text{-TMPP})_2][BF_4]_2$ (0.100 g, 0.07 mmol) and $[Cp_2Fe][BF_4]$ (0.014 g, 0.07 mmol) in 5 mL of CH_2Cl_2 was stirred at −40 °C for 30 min. The red solution was treated with 20 mL of diethyl ether to precipitate a solid; this was collected by filtration, washed with 2 × 10 mL of diethyl ether to remove ferrocene and finally dried in vacuo: yield 0.091 g (85%).

Demethylation of $[Rh(\eta^3\text{-TMPP})_2][BF_4]_3$: Formation of $[Rh(\eta^3\text{-TMPP})(P\{C_6H_2(OMe)_3\}_2\{C_6H_2(OMe)_2O\})][BF_4]_2$ (5). (i) Solution. A quantity of $[Rh(\eta^3\text{-TMPP})_2][BF_4]_3$ (0.150 g, 0.11 mmol) was dissolved in 10 mL of acetone to give a red solution which was stirred overnight at room temperature. The pale orange solution was filtered through Celite and treated with 20 mL of diethyl ether to produce an orange solid. The sample was collected by suction filtration, washed with 2 × 5 mL of diethyl ether, and dried under reduced pressure: yield 0.085 g (61%). Anal. Calcd for $C_{53}H_{63}F_8P_2O_{18}B_2Rh$: C, 47.98; H, 4.79. Found: C, 47.28; H, 5.21.

(ii) Solid State. An amount of $[Rh(\eta^3\text{-TMPP})_2][BF_4]_3$ (0.015 g, 0.01 mmol) was placed in a Schlenk tube and heated to 50 °C for 36 h in an oil bath, during which time the color of the solid changed from deep red to pale orange. After cooling to room temperature, the ^1H NMR spectrum of the solid was recorded and compared to an authentic sample of **5** prepared as in (i). Conversion of **2** to **5** was quantitative based on this result.

Reaction of $[Rh(\eta^3\text{-TMPP})_2][BF_4]_2$ (1) with CO. In a typical reaction, $[Rh(\eta^3\text{-TMPP})_2][BF_4]_2$ (0.100 g, 0.07 mmol) in 10 mL of CH_2Cl_2 was purged with CO gas for 20 min. While maintaining a CO atmosphere, 20 mL of CO-purged diethyl ether was added to the solution, which caused the separation of an oily red solid from a yellow solution. The solution was decanted from the solid, the volume of the solution was reduced to 5 mL, and diethyl ether (20 mL) was slowly added to precipitate a yellow microcrystalline solid. The product was filtered in air, washed with 2 × 10 mL of diethyl ether, and dried in vacuo: yield 0.038 g (40%). The red oil was dissolved in 5 mL of CH_2Cl_2 and layered with 20 mL of diethyl ether. The resulting red-orange precipitate was collected by filtration, washed with 3 × 5 mL diethyl ether, and dried in vacuo: yield 0.043 g (41%).

Reaction of $[Rh(\eta^3\text{-TMPP})_2][BF_4]_2$ (1) with $^{12}CO/^{13}CO$ (1:1). A quantity of $[Rh(\eta^3\text{-TMPP})_2][BF_4]_2$ (0.050 g, 0.035 mmol) was dissolved in 10 mL of methylene chloride, and the solution was degassed by several freeze/pump/thaw cycles on a high vacuum line. An equimolar volume of ^{12}CO and ^{13}CO was delivered to the reaction flask with the use of a Toepler pump. The pressure above the solution was calculated to be in the range of 1–2 atm at room temperature. The reaction vessel was allowed to slowly warm to room temperature, during which time the solution color changed from purple to murky red. After 30 min, a small amount of solution was syringed out, and its infrared spectrum was measured: ν(CO) (cm^{-1}) 2011, 1985, 1968 in an approximate 1:2:1 intensity ratio.

Preparation of $[Rh(\eta^2\text{-TMPP})(TMPP)CO][BF_4]$ (4). (i) Reduction of $[Rh(\eta^3\text{-TMPP})_2][BF_4]_2$ in the Presence of CO. A solution of $[Rh(\eta^3\text{-TMPP})_2][BF_4]_2$ (0.100 g, 0.07 mmol) and Cp_2Co (0.042 g, 0.22 mmol) in 5 mL of CH_2Cl_2 was stirred under a moderate purge of carbon monoxide. After 20 min, 30 mL of diethyl ether was added, and the solution was cooled to −5 °C for 24 h. The yellow product was collected by suction filtration, washed with diethyl ether, and recrystallized from CH_2Cl_2 (10 mL)/THF (5 mL) by reduction of the volume and slow addition of diethyl ether (0.5 mL). A crop of yellow-orange crystals was collected by filtration in air, washed with diethyl ether, and dried in vacuo: yield 0.057 g (60%). Anal. Calcd for $C_{55}H_{66}F_4P_2O_{19}BRh$: C, 51.50; H, 5.19. Found: C, 50.57; H, 5.02.

(ii) Reaction of $[Rh(cod)Cl]_2$ with TMPP in the Presence of CO. A mixture of $[Rh(cod)Cl]_2$ (0.100 g, 0.20 mmol) and $AgBF_4$ (0.079 g, 0.40 mmol) was stirred in 5 mL of THF for 5 min to give a yellow solution. The reaction solution was filtered through a Celite filter plug into a three-necked flask equipped with an addition funnel containing TMPP (0.432 g, 0.8 mmol) in 10 mL of CO-saturated THF at 0 °C. The THF solution was added dropwise over the period of several minutes at 0 °C, and the solution was stirred under a constant CO purge for 1 h. The crude product was precipitated by the addition of 50 mL of diethyl ether, filtered in air, and recrystallized in the manner described in method (i) above: yield 0.350 g (71%).

Preparation of $[Rh(TMPP)_2(CO)_2][BF_4]$ (3). A quantity of $[Rh(\eta^2\text{-TMPP})(TMPP)CO][BF_4]$ (0.100 g, 0.08 mmol) in 5 mL of CH_2Cl_2 was treated with CO gas for 5 min, after which time 30 mL of CO-saturated diethyl ether was slowly added to induce precipitation of the product. The yellow crystalline solid was collected by suction filtration in air, washed with 2 × 5 mL of diethyl ether, and dried. The product was isolated as the CH_2Cl_2 solvate: yield 0.10 g (90%). Anal. Calcd for $RhCl_2P_2C_{57}O_{20}BF_4H_{68}$: C, 49.05; H, 4.91. Found: C, 48.22; H, 4.96.

Solid-State Reactions of 1–4 with CO. In a typical experiment, a small amount of finely divided starting compound (5–10 mg) in a polyethylene vial was placed in a Parr reactor. After several fillings and subsequent purgings with CO, the reactor was pressurized to approximately 50 psi. Reaction times were varied from 15 min to 5 days. After the vessel was depressurized, a small drop of Nujol oil was added, and the sample was quickly transferred to CsI plates for infrared spectral measurements. Alternatively the reactions were performed by purging a finely divided sample suspended in Nujol with CO at atmospheric pressure for an extended period of time.

Reaction of $[Rh(\eta^2\text{-TMPP})(TMPP)CO][BF_4]$ (4) with $[Rh(\eta^3\text{-TMPP})_2][BF_4]_3$ (2). An equimolar mixture of $[Rh(TMPP)_2CO][BF_4]$ (4) (0.012 g, 0.009 mmol) and $[Rh(\eta^3\text{-TMPP})_2][BF_4]_3$ (2) (0.013 g, 0.009 mmol) was dissolved in 10 mL of CH_2Cl_2, and the reaction was stirred for 90 min under an argon purge to liberate CO. During this time, the solution color changed from red to red-purple. After stirring overnight under an Ar atmosphere, the solvent was evaporated, and a crop of purple crystals was collected, washed with a mixture of CH_2Cl_2/Et_2O (1:1 v/v), and dried in air. The product was identified as $[Rh(\eta^3\text{-TMPP})_2][BF_4]_2$ by a comparison of its electrochemical and infrared spectral properties to those of an authentic sample: yield 0.011 g (90% based on $[Rh(\eta^2\text{-TMPP})(TMPP)CO][BF_4]$ (4)).

Physical Measurements. Infrared spectra were recorded on a Perkin-Elmer 599 or a Nicolet 740 FT-IR spectrophotometer. ^1H NMR spectra were measured on a Varian 300-MHz or Varian 500-MHz spectrometer. Chemical shifts were referenced relative to the residual proton impurities of methylene-d_2 chloride (5.32 ppm with respect to TMS). $^{31}P\{^1H\}$ spectra were obtained on a Varian 300-MHz spectrometer operating at 121.4 MHz and were referenced relative to an external standard of 85% phosphoric acid. Electronic absorption spectra were measured on a Hitachi U-2000 or a Cary 17 spectrophotometer. Electrochemical measurements were performed by using an EG&G Princeton Applied Research Model 362 scanning potentiostat in conjunction with a BAS Model RXY recorder. Cyclic voltammetry experiments were carried out at 22 ± 2 °C in methylene chloride containing 0.1 M tetra-*n*-butylammonium tetrafluoroborate ($TBABF_4$) as the supporting electrolyte. $E_{1/2}$ values, determined as $(E_{p,a} + E_{p,c})/2$, were referenced to the Ag/AgCl electrode and are uncorrected for junction potentials. The Cp_2Fe/Cp_2Fe^+ couple occurs at $E_{1/2}$ = +0.46 V under the same experimental conditions. X-band EPR spectra were obtained by using a Bruker ER200D spectrometer. To obtain an accurate measure of g values and line widths, a Bruker ER035M NMR Gaussmeter and a Hewlett-Packard 5245L frequency counter (with a 3–12 GHz adaptor) were used to measure magnetic field strength and the microwave frequency, respectively. Variable-temperature and field magnetic susceptibility measurements were carried out on a 10 KG BTI Superconducting Quantum Interference Device (SQUID) at Michigan State University. Data points were collected over a temperature range from 5 to 286 K at 20 deg intervals in fields of 3, 5, and 7 KG. Additional solid-state magnetic susceptibility measurements were determined at room temperature by using a Johnson-Matthey magnetic susceptibility balance. Solution magnetic susceptibility measurements were carried out by application of the Evans method[18] on a Bruker WM 250 equipped with an Aspect 3000 computer. Elemental analyses were performed at Galbraith Laboratories, Inc.

X-ray Crystallographic Procedures. The structures of the complexes $[Rh(\eta^3\text{-TMPP})_2][BF_4]_2$ (1) and $[Rh(TMPP)_2(CO)_2][BF_4]$ (3) were

(18) (a) Evans, D. F. *J. Chem. Soc.* **1959**, 2003. (b) Deutsch, J. L.; Poling, S. M. *J. Chem. Ed.* **1969**, *46*, 167.

determined by application of general procedures fully described elsewhere.[19] Geometric and intensity data were collected on a Nicolet P3/F diffractometer with graphite monochromated Mo Kα ($\lambda\bar{\alpha}$ = 0.71073 Å) radiation and were corrected for Lorentz and polarization effects. Calculations for **1** and **3** were performed on a VAXSTATION 2000 computer by using programs from the Enraf-Nonius Structure Determination Package (SDP) programs.[20]

Crystallographic data for the compound [Rh(η^2-TMPP)(TMPP)-CO][BF_4] (**4**) were collected on a Rigaku AFC5R diffractometer with monochromated Cu Kα radiation and a 12 KW rotating anode generator. Calculations were performed by using the Texsan crystallographic software package of Molecular Structure Corporation.[21]

[Rh(η^3-TMPP)$_2$][BF_4]$_2$ (1). Single crystals of **1** were grown by a careful layering of toluene on a solution of the compound in CH_2Cl_2. A red-purple parallelpiped with approximate dimensions 0.67 × 0.35 × 0.22 mm^3 was mounted on the tip of a glass fiber with epoxy cement. Geometric and intensity data were collected at 22 ± 2 °C. Indexing and refinement of 16 reflections in the range $4 \le 2\theta \le 12°$ selected from a rotational photograph gave unit cell parameters for an orthorhombic crystal system. The cell was further refined by a least-squares fit of 20 reflections in the range of $13 \le 2\theta \le 25°$. The Laue class was determined to be *mmm* by axial photography. A total of 3952 unique data were collected in the range $4 \le 2\theta \le 45°$ by using the θ–2θ scan technique. Three standard reflections, measured at regular intervals every 97 reflections, decayed by 2%; a decay correction was applied to the data by using the program CHORT in SDP. After data reduction, a total of 2462 reflections remained with $F_o^2 > 3\sigma(F_o^2)$. The position of the Rh atom was located by the direct methods program in SHELXS-86. The remaining non-hydrogen atoms were located through successive cycles of least-squares refinements and difference Fourier maps. After convergence was reached with isotropic thermal parameters, an absorption correction based upon the program DIFABS was applied to the data.[22] In the end, refinement of 369 parameters gave residuals of R = 0.073 and R_w = 0.089 and a quality-of-fit index of 2.37. The largest shift/esd was 0.58 and the highest peak in the final difference Fourier map was 1.91 e$^-$/Å^3.

[Rh(TMPP)$_2$(CO)$_2$][BF_4]·CH_2Cl_2 (3). Single crystals of **3** that were suitable for X-ray diffraction studies were grown by slow vapor diffusion of Et_2O into a CH_2Cl_2 solution of **3** under a carbon monoxide atmosphere to prevent loss of CO and formation of **4**. A yellow platelet of approximate dimensions 0.89 × 1.0 × 0.37 mm^3 was taken up in viscous oil at the end of a glass fiber and placed in a cold stream of N_2(g) at −96 ± 3 °C. The cell parameters were refined from a fit of 15 reflections in the range $20 \le 2\theta \le 30°$ and indicated a triclinic crystal system; axial photography confirmed the low symmetry of the lattice. A total of 8801 unique data were collected in the range $4 \le 2\theta \le 45°$ by using the ω-scan method. No significant decay in the data was noted, as evidenced by three check reflections that were monitored periodically throughout data collection. The position of the Rh atom was determined from a Patterson Fourier synthesis. The remaining non-hydrogen atoms were located and refined by a series of alternating least-squares cycles and difference Fourier maps. Of the 8801 unique data, 5934 with $F_o^2 > 3\sigma(F_o)^2$ were used in the refinement of 799 parameters to give residuals of R = 0.059 and R_w = 0.084 and a quality-of-fit index of 2.32. The largest shift/esd was 0.82 and the highest peak in the final differences Fourier map was 0.683 e$^-$/Å^3.

[Rh(η^2-TMPP)(TMPP)CO][BF_4]·2C_6H_6 (4). Yellow platelets of **4** were grown by slow evaporation of a mixture of CH_2Cl_2 and C_6H_6. A small crystal of approximate dimensions 0.25 × 0.10 × 0.10 mm^3 was selected and mounted on the end of a glass fiber with epoxy cement. Least-squares refinement of 25 well-centered reflections in the range $58.5 \le 2\theta \le 77.2°$ gave cell parameters that belong to a triclinic cell. On the basis of an analysis of intensities, the space group was determined to be $P\bar{1}$. Data were collected at 23 ± 1 °C by using the ω-2θ scan technique to a maximum 2θ value of 120.3°. Weak reflections, those with $F_o^2 < 10\sigma(F_o^2)$, were rescanned at a maximum of two rescans, and the counts were accumulated to assure good counting statistics. A total of 10304 reflections were collected, of which 9855 were unique. Intensity measurements of three standard reflections every 150 data points indicated that the crystal had not decayed. An empirical absorption correction based upon azimuthal scans of several reflections was applied to the data; transmission factors ranged from 1.00 to 0.95. Data were also corrected for Lorentz and polarization effects. The structure was solved by MITHRIL and DIRDIF structure solution programs[23] and refined by full-matrix least-squares refinement. With the exception of the carbon atoms of the benzene molecule in the lattice, all non-hydrogen atoms were refined with anisotropic thermal parameters. A total of 6393 observations with $F_o^2 > 3\sigma(F_o^2)$ were used to fit 757 parameters to give R = 0.067 and R_w = 0.069. The quality-of-fit index is 2.59, and the peak of highest electron density in the final difference map was 1.09 e$^-$/Å^3.

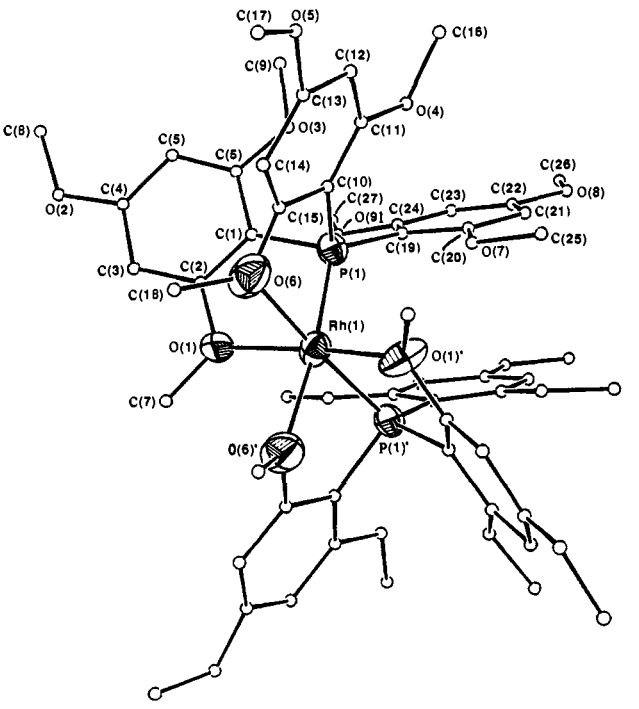

Figure 1. ORTEP representation of [Rh(η^3-TMPP)$_2$]$^{2+}$ (**1**) molecular cation with 40% probability ellipsoids. Phenyl ring atoms are shown as small spheres of arbitrary size for clarity.

Results

The highly unusual mononuclear rhodium(II) complex, [Rh(η^3-TMPP)$_2$][BF_4]$_2$ (**1**), was isolated in high yield, and although the cation possesses extraordinarily air and thermal stability for a radical species, it nonetheless exhibits a rich and varied chemistry. Chemical or electrochemical oxidation of **1** produces the d^6 Rh(III) complex [Rh(η^3-TMPP)$_2$][BF_4]$_3$ (**2**) with a ligand arrangement identical to that found in the parent complex. In striking contrast to the remarkable stability of the divalent complex [Rh(η^3-TMPP)$_2$][BF_4]$_2$ (**1**), the Rh(III) species **2** is air-sensitive and thermally unstable, eventually forming the demethylated complex Rh(III) complex, [Rh(η^3-TMPP)(P{C_6H_2(OMe)$_3$}$_2$-{C_6H_2(OMe)$_2$O}][BF_4]$_2$ (**5**).

[Rh(η^3-TMPP)$_2$][BF_4]$_2$ (**1**) reacts with carbon monoxide under mild conditions to initiate a series of electron-transfer reactions which involve the formation of two Rh(I) carbonyl complexes, [Rh(TMPP)$_2$(CO)$_2$][BF_4] (**3**) and [Rh(η^2-TMPP)(TMPP)-CO][BF_4] (**4**), in addition to the Rh(III) complex (**2**). Upon purging the reaction solution with an inert gas, the original Rh(II) species is regenerated in quantitative yields. For the purpose of fully understanding this chemistry, compounds **2**–**5** have been synthesized by independent high-yield methods and characterized by infrared, ^{1}H NMR, ^{31}P NMR, electronic spectroscopy, and cyclic voltammetry. The results of these studies are presented in Tables I and II. The paramagnetism of **1** was investigated by EPR spectroscopy and magnetic susceptibility, the results of which are presented in Table III. The structures of compounds **1**, **2**, **3**, and **4** have been determined by single-crystal X-ray diffraction methods. Crystal parameters and basic information

(19) (a) Bino, A.; Cotton, F. A.; Fanwick, P. E. *Inorg. Chem.* **1979**, *18*, 3558. (b) Cotton, F. A.; Frenz, B. A.; Deganello, G.; Shaver, A. *J. Organomet. Chem.* **1973**, 227.

(20) SDP: Structure Determination Package, Enraf-Nonius, Delft, The Netherlands, 1979.

(21) TEXSAN–TEXRAY Structure Analysis Package, Molecular Structure Corporation, 1985.

(22) Walker, N.; Stuart, D. *Acta Crystallogr.* **1983**, *A39*, 158.

(23) MITHRIL: Integrated Direct Methods Computer Program, Gilmore, C. J. *J. Appl. Cryst.* **1984**, *17*, 42. DIRDIF: Direct Methods for Difference Structure, An Automatic Procedure for Phase Extension; Refinement of Difference Structure Factors. Beurskens, R. T. Technical Report, 1984.

Table I. NMR Spectroscopic Data for **1–5**

compound	^{1}H NMR spectra,[a] ppm	^{31}P NMR spectra,[b] ppm	^{31}P NMR coupling constants, Hz
1, $[Rh(\eta^3\text{-TMPP})_2][BF_4]_2$	3.2, 4.7 (very br)	not observed	not observed
2, $[Rh(\eta^3\text{-TMPP})_2][BF_4]_3$	O-Me: 2.93 (s, 6 H), 3.57 (s, 6 H), 3.59 (s, 6 H), 3.64 (s, 6 H) 3.90 (s, 6 H), 3.92 (s, 6 H), 3.97 (s, 6 H), 4.19 (s, 6 H) 4.69 (s, 6 H) meta: 5.73 (dd, 2 H), 6.05 (dd, 2 H), 6.18 (dd, 2 H) 6.32 (dd, 2 H), 6.50 (dd, 2 H), 6.68 (dd, 2 H)	37.4 (d)	$^1J_{Rh-P}$ = 107
3, $[Rh(TMPP)_2(CO)_2][BF_4]$	O-Me: 3.41 (s, 18 H), 3.79 (s, 36 H) meta: 6.02 (t, 12 H)	−23.8 (d)	$^1J_{Rh-P}$ = 116
4, $[Rh(\eta^2\text{-TMPP})(TMPP)(CO)][BF_4]$	O-Me: 3.48 (s, 18 H), 3.80 (s, 36 H) meta: 6.04 (s, 12 H)	−11.1 (d)	$^1J_{Rh-P}$ = 128
5, $[Rh(\eta^3\text{-TMPP})(\eta^3\text{-TMPP-}O)][BF_4]_2$	O-Me: 2.94 (s, 3 H), 3.06 (s, 3 H), 3.32 (s, 3 H), 3.41 (s, 3 H) 3.46 (s, 3 H), 3.52 (s, 3 H), 3.53 (s, 3 H), 3.55 (s, 3 H) 3.68 (s, 3 H), 3.84 (s, 3 H), 3.85 (s, 6 H), 3.90 (s, 3 H) 3.92 (s, 3 H), 4.16 (s, 3 H), 4.33 (s, 3 H), 4.51 (s, 3 H) meta: 5.60 (mult, 3 H), 5.84 (dd, 1 H), 4.89 (dd, 1 H) 5.98 (dd, 1 H), 6.11 (dd, 1 H), 6.19 (dd, 1 H) 6.23 (dd, 1 H), 6.36 (dd, 1 H), 6.53 (dd, 1 H) 6.96 (dd, 1 H)	31.5 (dd) 37.9 (dd)	$^1J_{Rh-P_A}$ = 140 $^1J_{Rh-P_B}$ = 139 $^2J_{P_A-P_B}$ = 13.7

[a] δ in CD_2Cl_2. [b] δ in CD_2Cl_2, relative to 85% H_3PO_4.

Table II. Electrochemical and Electronic Absorption Data for Compounds **1–5**

compound	cyclic voltammetry potentials,[a] V		electronic abs spectra λ_{max},[b] nm (ϵ)
1, $[Rh(\eta^3\text{-TMPP})_2][BF_4]_2$	$E_{1/2(ox)}$ = +0.46	$E_{1/2(red)}$ = −0.65	537 (2050), 420 sh, 329 (13 400) 298 (17 500), 233 (62 400)
2, $[Rh(\eta^3\text{-TMPP})_2][BF_4]_3$	$E_{1/2(red)(1)}$ = +0.46	$E_{1/2(red)(2)}$ = −0.65	363 (22 000), 260 sh 245 (65 000)
3, $[Rh(TMPP)_2(CO)_2][BF_4]$	$E_{p,a}$ = +0.80		438 (3400), 350 (6400) 288 sh, 256 (61 500)
4, $[Rh(\eta^2\text{-TMPP})(TMPP)(CO)][BF_4]$	$E_{1/2(ox)}$ = +0.50		415 sh, 345 (7770), 305 sh 285 sh, 254 (64 400)
5, $[Rh(\eta^3\text{-TMPP})(\eta^3\text{-TMPP-}O)][BF_4]_2$	$E_{p,a}$ = +1.55	$E_{p,c}$ = −0.80 $E_{p,a}$ = −0.02	329 (25 000), 260 sh 242 sh

[a] Electrochemical measurements in 0.1 M $[(n\text{-Bu})_4N][BF_4]$–CH_2Cl_2 solution, at a Pt disk electrode referenced to Ag/AgCl. [b] CH_2Cl_2 solution (2×10^{-4}–1×10^{-3} M).

Table III. EPR Spectroscopic and Magnetic Susceptibility Data for $[Rh(\eta^3\text{-TMPP})_2][BF_4]_2$ (**1**)

	$[Rh(\eta^3\text{-TMPP})_2][BF_4]_2$ (**1**)
EPR (CH_2Cl_2/Me–THF glass)[a]	
g_{xx}	2.26
g_{yy}	2.30
g_{zz}	1.99
A_{zz}, G (cm^{-1})	22 (2.0×10^{-3})
magnetic moment,[b] μ_{eff}, μ_B	
solution[c]	2.10
solid[d]	1.80

[a] Measured at 77 K. [b] A diamagnetic correction of -724×10^{-6} was applied based on -20×10^{-6} for Rh^{2+}, -39×10^{-6} for BF_4^-, and -313×10^{-6} for TMPP. [c] Measured in CH_2Cl_2 at 294 K using Evans method.[18] [d] Average magnetic moment measured over a temperature range of 5–286 K at several field strengths.

pertaining to data collection and structure refinement are summarized in Table IV. ORTEP representations of $[Rh(\eta^3\text{-TMPP})_2][BF_4]_2$ (**1**), $[Rh(TMPP)_2(CO)_2][BF_4]$ (**3**), and $[Rh(\eta^2\text{-TMPP})(TMPP)CO][BF_4]$ (**4**) are depicted in Figures 1–4. Selected bond distances and angles for each structure are listed in Tables V, VI, and VII. Full tables of positional and anisotropic thermal parameters and complete listings of all bond distances and angles for compounds **1**, **2**, **3**, and **4** are available as supplementary material. The interpretation of these results and the relationship of these five compounds to the key reaction in this

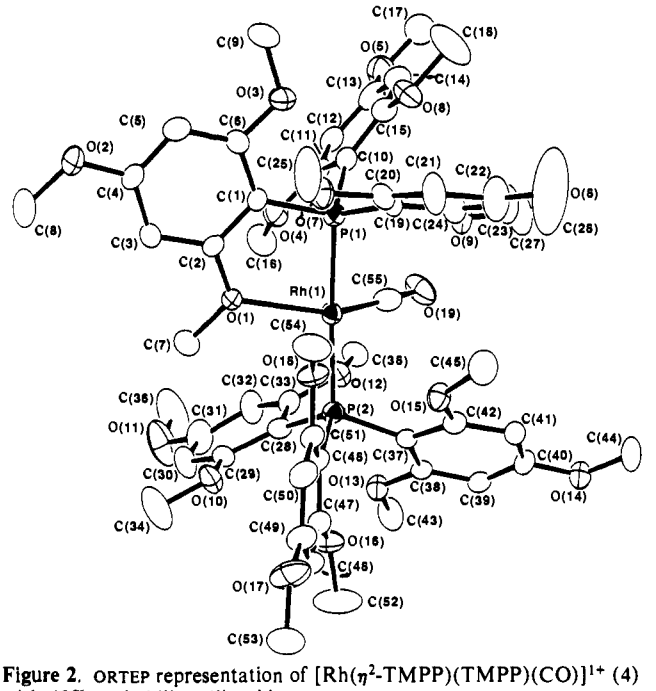

Figure 2. ORTEP representation of $[Rh(\eta^2\text{-TMPP})(TMPP)(CO)]^{1+}$ (**4**) with 40% probability ellipsoids.

Table IV. Summary of Crystallographic Data for $[Rh(\eta^3\text{-TMPP})_2][BF_4]_2$ (**1**), $[Rh(TMPP)_2(CO)_2][BF_4]\cdot CH_2Cl_2$ (**3**), and $[Rh(\eta^2\text{-TMPP})(TMPP)(CO)][BF_4]\cdot 2C_6H_6$ (**4**) (**4**)

	1	**3**	**4**
formula	$RhP_2F_8O_{18}C_{54}B_2H_{66}$	$RhCl_2P_2F_4O_{20}C_{57}BH_{68}$	$RhP_2F_4O_{19}C_{67}BH_{78}$
formula wt	1341.5	1395.73	1432.02
space group	*Pbcn*	*P* − 1	*P* − 1
a, Å	15.938 (5)	13.318 (4)	14.898 (5)
b, Å	17.916 (7)	13.404 (2)	18.060 (8)
c, Å	21.015 (8)	18.164 (4)	14.343 (4)
α, deg	90	95.908 (3)	96.56 (4)
β, deg	90	97.037 (3)	113.84 (2)
γ, deg	90	90.711 (3)	104.80 (4)
V, Å^3	6001 (6)	3200 (2)	3308 (2)
Z	4	2	2
d_{calc}, g/cm^3	1.427	1.448	1.438
μ, cm^{-1}	4.20	4.74	32.60
radiation (monochromated in incident beam)	Mo Kα (λ_α = 0.71073 Å) graphite monochromated	Mo Kα (λ_α = 0.71073 Å) graphite monochromated	Cu Kα (λ = 1.54178 Å)
temp, °C	22 ± 2	−96 ± 3	23 ± 1
trans factors, max., min.	1.00, 0.87	1.00, 0.82	1.00, 0.95
R^a	0.073	0.059	0.067
$R_w{}^b$	0.089	0.084	0.069

$^a R = \sum||F_o| - |F_c||/\sum|F_o|$. $^b R_w = [\sum w|F_o| - |F_c|)^2/\sum w|F_o|^2]^{1/2}$; $w = 1/\sigma^2(|F_o|)$.

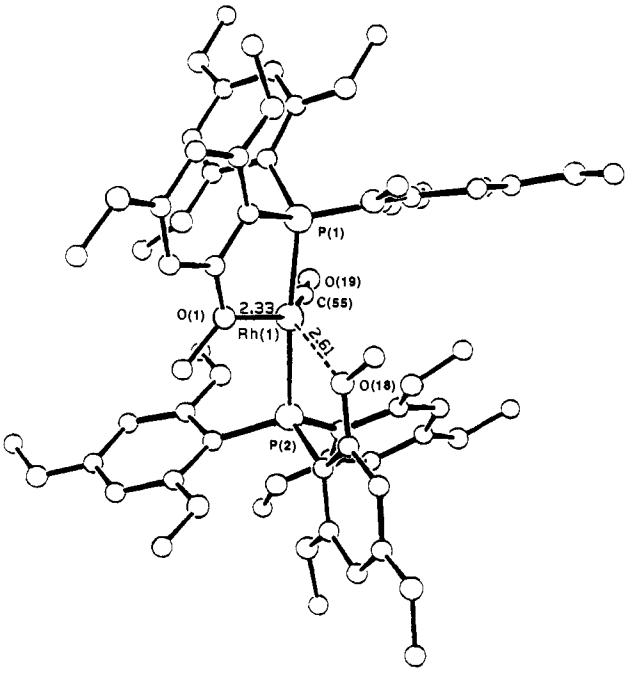

Figure 3. PLUTO drawing of $[Rh(\eta^2\text{-TMPP})(TMPP)(CO)]^{1+}$ (**4**) emphasizing the coordination geometry about rhodium.

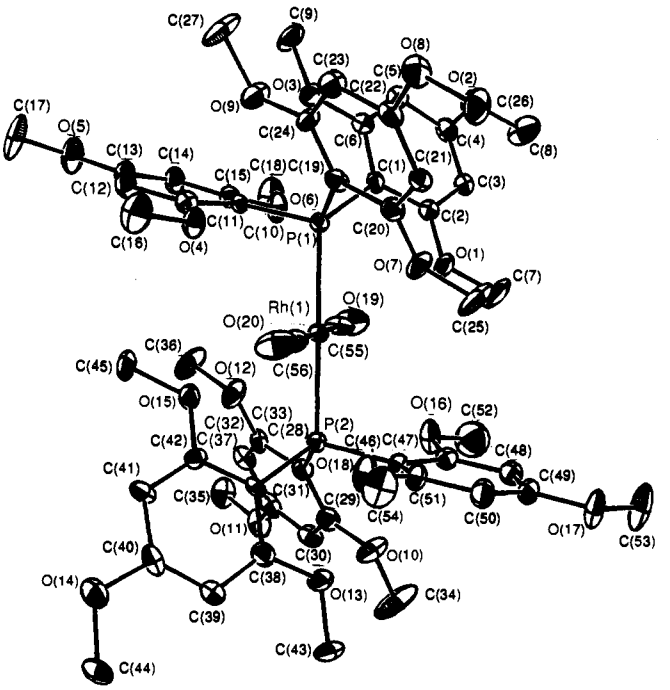

Figure 4. ORTEP drawing of $[Rh(TMPP)_2(CO)_2]^{1+}$ (**3**) with 30% probability ellipsoids.

study are discussed in the following sections.

Preparation and Spectroscopic Properties of $[Rh(\eta^3\text{-TMPP})_2][BF_4]_2$ (1). Slow addition of TMPP to $[Rh_2(CH_3CN)_{10}][BF_4]_4$, both dissolved in CH_3CN, immediately produces a dark red-purple solution of **1**, with the reaction being complete within 15 min. The product must be isolated immediately, as a side-reaction occurs involving demethylation of one of the coordinated methoxy groups by free phosphine if **1** is allowed to remain in solution. This results in the formation of a new Rh(II) complex which we believe is ligated by one neutral TMPP ligand and a phenoxyphosphine derivative of TMPP as judged by the formation of the methylphosphonium salt of TMPP, $[(C_6H_2(OMe)_3)_3PCH_3][BF_4]$, easily characterized by ^1H NMR and IR spectroscopy. Unlike **1**, the demethylated Rh(II) complex is air-sensitive and readily decomposes to an intractable mixture of diamagnetic species. Details of the deliberate synthesis of this species by reaction of **1** with various nucleophiles will be published in due course.[24]

Compound **1** was also synthesized by addition of a methanolic solution of TMPP to a suspension of $[Rh_2(CH_3CN)_{10}][BF_4]_4$ in MeOH, but the yields are not as high as the reaction in CH_3CN; this is presumably due to the low solubility of the Rh_2^{4+} salt in MeOH which serves to keep the phosphine ligand in excess and increases the likelihood of the demethylation side reaction. This work is ongoing and will be treated in full elsewhere. As a final synthetic approach to $[Rh(\eta^3\text{-TMPP})_2][BF_4]_2$ or to a chloride derivative of the complex, we reacted TMPP with $RhCl_3\cdot xH_2O$ in refluxing ethanol, a method that has been widely used to prepare many of the reported Rh(II) species with bulky phosphines.[11] In the present case, however, a complex mixture of diamagnetic products was detected by ^1H NMR spectroscopy. We rationalize that this is largely due to the instability of $[Rh(\eta^3\text{-TMPP})_2][BF_4]_2$ in the presence of free halides.

The compound $[Rh(\eta^3\text{-TMPP})_2][BF_4]_2$ is soluble in methylene chloride and acetonitrile, partially soluble in methanol and chloroform, and completely insoluble in water, tetrahydrofuran, diethyl ether, and hydrocarbon solvents. Remarkably, the complex is air-stable, but CH_2Cl_2 solutions decompose slowly within several

(24) Dunbar, K. R.; Haefner, S. C., unpublished results.

Table V. Selected Bond Distances (Å) and Bond Angles (deg) for $[Rh(\eta^3\text{-TMPP})_2][BF_4]_2$ (**1**)

Bond Distances

atom 1	atom 2	distance	atom 1	atom 2	distance	atom 1	atom 2	distance
Rh(1)	P(1)	2.216 (2)	O(3)	C(9)	1.449 (8)	C(2)	C(3)	1.38 (1)
Rh(1)	O(1)	2.398 (5)	O(4)	C(11)	1.37 (1)	C(3)	C(4)	1.40 (1)
Rh(1)	O(6)	2.201 (6)	O(4)	C(16)	1.48 (1)	C(4)	C(5)	1.37 (1)
P(1)	C(1)	1.829 (7)	O(6)	C(15)	1.39 (1)	C(5)	C(6)	1.39 (1)
P(1)	C(10)	1.826 (7)	O(6)	C(18)	1.45 (1)	C(10)	C(11)	1.38 (1)
P(1)	C(19)	1.770 (7)	O(7)	C(20)	1.351 (9)	C(10)	C(15)	1.41 (1)
O(1)	C(2)	1.393 (9)	O(7)	C(25)	1.49 (1)	C(14)	C(15)	1.42 (1)
O(1)	C(7)	1.470 (9)	O(9)	C(24)	1.367 (8)	C(19)	C(20)	1.42 (1)
O(2)	C(4)	1.380 (9)	O(9)	C(27)	1.445 (9)	C(19)	C(24)	1.41 (1)
O(2)	C(8)	1.44 (1)	C(1)	C(2)	1.39 (1)			
O(3)	C(6)	1.370 (8)	C(1)	C(6)	1.41 (1)			

Bond Angles

atom 1	atom 2	atom 3	angle	atom 1	atom 2	atom 3	angle	atom 1	atom 2	atom 3	angle
P(1)	Rh(1)	P(1)′	105.2 (1)	C(4)	O(2)	C(8)	118.8 (7)	C(4)	C(5)	C(6)	116.5 (7)
P(1)	Rh(1)	O(1)	80.5 (1)	C(6)	O(3)	C(9)	119.6 (6)	O(3)	C(6)	C(1)	114.1 (7)
P(1)	Rh(1)	O(1)′	107.1 (1)	C(11)	O(4)	C(16)	120.5 (8)	O(3)	C(6)	C(5)	123.1 (7)
P(1)	Rh(1)	O(6)	77.9 (2)	Rh(1)	O(6)	C(15)	113.9 (5)	C(1)	C(6)	C(5)	122.8 (7)
P(1)	Rh(1)	O(6)′	171.5 (2)	C(15)	O(6)	C(18)	118.5 (7)	P(1)	C(10)	C(11)	129.8 (8)
O(1)	Rh(1)	O(1)′	167.8 (3)	C(20)	O(7)	C(25)	118.3 (6)	P(1)	C(10)	C(15)	113.0 (7)
O(1)	Rh(1)	O(6)	91.1 (2)	C(24)	O(9)	C(27)	117.3 (6)	C(11)	C(10)	C(15)	117.2 (9)
O(1)	Rh(1)	O(6)′	81.1 (2)	P(1)	C(1)	C(2)	122.1 (6)	O(4)	C(11)	C(10)	117.4 (8)
O(6)	Rh(1)	O(6)′	100.2 (3)	P(1)	C(1)	C(6)	120.7 (6)	O(6)	C(15)	C(10)	116.3 (8)
Rh(1)	P(1)	C(1)	102.9 (3)	C(2)	C(1)	C(6)	116.7 (7)	O(6)	C(15)	C(14)	119 (1)
Rh(1)	P(1)	C(10)	99.6 (3)	O(1)	C(2)	C(1)	115.6 (6)	C(10)	C(15)	C(14)	124 (1)
Rh(1)	P(1)	C(19)	124.5 (3)	O(1)	C(2)	C(3)	120.8 (7)	P(1)	C(19)	C(20)	117.2 (6)
C(1)	P(1)	C(10)	100.8 (3)	C(1)	C(2)	C(3)	123.4 (7)	P(1)	C(19)	C(24)	126.4 (6)
C(1)	P(1)	C(19)	113.5 (4)	C(2)	C(3)	C(4)	116.3 (7)	C(20)	C(19)	C(24)	116.4 (7)
C(10)	P(1)	C(19)	112.3 (4)	O(2)	C(4)	C(3)	112.7 (7)	O(7)	C(20)	C(19)	113.4 (7)
Rh(1)	O(1)	C(2)	113.8 (4)	O(2)	C(4)	C(5)	123.2 (7)	O(9)	C(24)	C(19)	116.5 (7)
C(2)	O(1)	C(7)	117.1 (6)	C(3)	C(4)	C(5)	124.1 (7)				

weeks; solid samples are stable for indefinite periods in air. These observations are somewhat surprising considering the documented, sensitive nature of mononuclear Rh(II) complexes. Typically these molecules can only be synthesized by electrochemical methods and subsequently decompose within short periods of time even under anaerobic conditions.[12a-c,25]

The infrared spectrum of $[Rh(\eta^3\text{-TMPP})_2][BF_4]_2$ displays bands assignable to coordinated TMPP ligands and a broad feature at 1050 cm^{-1} which is indicative of the BF_4^- counterion. The electronic spectrum recorded in CH_2Cl_2 exhibits a d–d transition at λ_{max} = 537 nm (2050 M^{-1} cm^{-1}) which is responsible for the intense purple color of the compound. Several higher energy charge-transfer transitions are located at λ_{max} = 329 nm (1.34×10^4 M^{-1} cm^{-1}), 298 nm (1.53×10^4 M^{-1} cm^{-1}), 285 nm (1.75×10^4 M^{-1} cm^{-1}), 233 nm (6.24×10^4 M^{-1} cm^{-1}).

Not unexpectedly for a d^7 metal complex, the ^1H and ^{31}P NMR signals are broad and reveal no information about the structure. In general, Rh(II) phosphine complexes have been characterized by their EPR activity and their broad, largely unidentifiable NMR features. We note that this data and ours are in sharp contrast to several puzzling instances in which paramagnetic Rh(II) compounds have evidently exhibited sharp and unshifted NMR signals as well as EPR signals.[12e,26]

Magnetic and EPR Spectroscopic Properties of $[Rh(\eta^3\text{-TMPP})_2][BF_4]_2$ (1). EPR measurements of **1** were carried out in a variety of solvents at room temperature and 77 K. Solutions of **1** in CH_2Cl_2, acetonitrile/toluene (1:1), and CH_2Cl_2/Me–THF (1:1) produced identical spectra at room temperature with a single isotropic homogeneous line at $g \approx 2.20$. At 77 K in the solvent mixtures, which form glasses at this temperature, a rhombic signal was observed (Figure 5). The g values of the CH_2Cl_2/Me-THF system are g_{xx} = 2.26, g_{yy} = 2.30, and g_{zz} = 1.99. The average of the three anisotropic g values equals that of the isotropic line at room temperature; therefore, the change in line shape is due to the rapid tumbling of the complex in solution, as opposed to being frozen in random orientations with respect to the applied field at 77 K. There is no evidence for a dynamic Jahn–Teller effect based on these data.[27] In the anisotropic spectrum (77 K), g_{zz} is split into a doublet due to the hyperfine interaction with the $I = 1/2$ nucleus of Rh. Other lines (g_{xx}, g_{yy}) do not split since their line widths are broader than the hyperfine tensor components along these axes. This feature is also observed with Co(II) and Fe(I). The hyperfine component along g_{zz} is interpreted as A_{zz}, and its value is 22 G for the CH_2Cl_2/Me–THF sample. Goldfarb and Kevan have published several papers on Rh(II) trapped onto zeolite surfaces;[28] they observed similar behavior as found in the present study, with g values differing slightly, which is reasonable considering that our sample is in a glass of organic solvents. In the zeolite study, a doublet splitting of g_{zz} of ~32 G was reported, and a dynamic Jahn–Teller effect was observed at high temperatures (400 °C).

The magnetic moment of $[Rh(\eta^3\text{-TMPP})_2][BF_4]_2$ (**1**) was measured both in solution and the solid state. The results of these studies are listed in Table III. Solid-state susceptibility measurements were performed over a temperature range of 5–286 K at a variety of field strengths. Compound **1** exhibits Curie-Weiss behavior over the entire range of temperatures. A plot of χ_m vs $1/T$ yielded a temperature independent paramagnetism (TIP) contribution of 424×10^{-6} cgsu, which was applied along with a correction for diamagnetism, to the average magnetic moment giving a value of 1.80 (3) μ_B. Solution studies were carried out using the Evans NMR method[18] and resulted in a μ_{eff} of 2.10 μ_B. Both measurements are consistent with the $S = 1/2$ ground state, as is expected for a low-spin d^7 ion. Similar values have been

(25) Examples of electrochemically prepared Rh(II) complexes. (a) Piloni, G.; Schiavon, G.; Zotti, G.; Zecchin, S. *J. Organomet. Chem.* **1977**, *134*, 305. (b) Anderson, J. E.; Gregory, T. P. *Inorg. Chem.* **1989**, *28*, 3905. (c) Rawle, S. C.; Yagbasan, R.; Prout, K.; Cooper, S. R. *J. Am. Chem. Soc.* **1987**, *109*, 6181. (d) Schwarz, H. A.; Creutz, C. *Inorg. Chem.* **1983**, *22*, 707. (e) Mulazzani, Q. G.; Emmi, S.; Hoffman, M. Z.; Venturi, M. *J. Am. Chem. Soc.* **1981**, *103*, 3362. (f) Bianchini, C.; Laschi, F.; Ottaviani, M. F.; Peruzzini, M.; Zanello, P.; Zanobini, F. *Organometallics* **1989**, *8*, 893. (g) Bianchini, C.; Meli, A.; Laschi, F.; Vizza, F.; Zanello, P. *Inorg. Chem.* **1989**, *28*, 227.

(26) Ogle, C. A.; Masterman, T. C.; Hubbard, J. L. *J. Chem. Soc., Chem. Commun.* **1990**, 1733.

(27) Abraham, A.; Bleaney, B. *Electron Paramagnetic Resonance of Transition Ions*; Clarendon Press: Oxford, 1970.

(28) Goldfarb, D.; Kevan, L. *J. Phys. Chem.* **1986**, *90*, 264, 2137, 5787.

Table VI. Selected Bond Distances (Å) and Bond Angles (deg) for $[Rh(TMPP)_2(CO)_2][BF_4]\cdot CH_2Cl_2$ (**3**)

Bond Distances

atom 1	atom 2	distance	atom 1	atom 2	distance	atom 1	atom 2	distance
Rh(1)	P(1)	2.327 (1)	O(1)	C(7)	1.391 (7)	C(4)	C(5)	1.412 (8)
Rh(1)	P(2)	2.332 (1)	O(2)	C(4)	1.374 (6)	C(5)	C(6)	1.396 (8)
Rh(1)	C(55)	1.906 (6)	O(2)	C(8)	1.451 (8)	C(10)	C(11)	1.370 (7)
Rh(1)	C(56)	1.898 (6)	O(3)	C(6)	1.356 (6)	C(10)	C(15)	1.395 (7)
P(1)	C(1)	1.828 (5)	O(3)	C(9)	1.433 (6)	C(19)	C(20)	1.434 (7)
P(1)	C(10)	1.839 (5)	O(19)	C(55)	1.125 (6)	C(19)	C(24)	1.395 (7)
P(1)	C(19)	1.843 (5)	O(20)	C(56)	1.145 (6)	C(37)	C(38)	1.405 (7)
P(2)	C(28)	1.823 (5)	C(1)	C(2)	1.409 (7)	C(37)	C(42)	1.413 (7)
P(2)	C(37)	1.829 (5)	C(1)	C(6)	1.395 (7)	C(46)	C(47)	1.383 (7)
P(2)	C(46)	1.825 (5)	C(2)	C(3)	1.406 (7)	C(46)	C(51)	1.405 (7)
O(1)	C(2)	1.355 (6)	C(3)	C(4)	1.389 (7)			

Bond Angles

atom 1	atom 2	atom 3	angle	atom 1	atom 2	atom 3	angle	atom 1	atom 2	atom 3	angle
P(1)	Rh(1)	P(2)	178.46 (6)	C(37)	P(2)	C(46)	110.0 (2)	C(6)	O(3)	C(9)	120.7 (4)
P(1)	Rh(1)	C(55)	91.7 (2)	P(1)	C(1)	C(2)	122.2 (4)	O(1)	C(2)	C(1)	116.4 (5)
P(1)	Rh(1)	C(56)	88.5 (2)	P(1)	C(1)	C(6)	121.4 (4)	O(1)	C(2)	C(3)	120.1 (5)
P(2)	Rh(1)	C(55)	89.9 (2)	C(2)	C(1)	C(6)	116.3 (5)	C(1)	C(2)	C(3)	123.6 (5)
P(2)	Rh(1)	C(56)	89.9 (2)	C(2)	C(3)	C(4)	116.3 (5)	P(2)	C(37)	C(38)	122.7 (4)
C(55)	Rh(1)	C(56)	179.0 (3)	O(2)	C(4)	C(3)	122.9 (5)	P(2)	C(37)	C(42)	120.8 (4)
Rh(1)	P(1)	C(1)	116.9 (2)	O(2)	C(4)	C(5)	113.6 (5)	C(38)	C(37)	C(42)	116.6 (5)
Rh(1)	P(1)	C(10)	101.8 (2)	C(3)	C(4)	C(5)	123.6 (5)	P(2)	C(46)	C(47)	122.0 (4)
Rh(1)	P(1)	C(19)	119.5 (2)	C(4)	C(5)	C(6)	116.6 (5)	P(2)	C(46)	C(51)	121.5 (4)
C(1)	P(1)	C(10)	108.2 (2)	O(3)	C(6)	C(1)	115.1 (5)	C(47)	C(46)	C(51)	115.6 (5)
C(1)	P(1)	C(19)	100.6 (2)	O(3)	C(6)	C(5)	121.4 (5)	P(2)	C(28)	C(29)	126.2 (4)
C(10)	P(1)	C(19)	109.6 (2)	C(1)	C(6)	C(5)	123.6 (5)	P(2)	C(28)	C(33)	117.5 (4)
Rh(1)	P(2)	C(28)	119.2 (2)	P(1)	C(10)	C(11)	121.8 (4)	C(29)	C(28)	C(33)	116.1 (5)
Rh(1)	P(2)	C(37)	115.2 (2)	P(1)	C(10)	C(15)	121.2 (4)	Rh(1)	C(55)	O(19)	179.2 (5)
Rh(1)	P(2)	C(46)	101.0 (2)	C(11)	C(10)	C(15)	116.7 (5)	Rh(1)	C(56)	O(20)	178.4 (5)
C(28)	P(2)	C(37)	101.5 (2)	C(2)	O(1)	C(7)	119.8 (5)				
C(28)	P(2)	C(46)	109.9 (2)	C(4)	O(2)	C(8)	116.7 (5)				

Table VII. Selected Bond Distances (Å) and Bond Angles (deg) for $[Rh(TMPP)_2(CO)][BF_4]\cdot 2(C_6H_6)$ (**4**)

Bond Distances

atom 1	atom 2	distance	atom 1	atom 2	distance	atom 1	atom 2	distance
Rh(1)	P(1)	2.316 (3)	O(1)	C(7)	1.43 (1)	C(10)	C(11)	1.41 (1)
Rh(1)	P(2)	2.354 (3)	O(2)	C(4)	1.36 (2)	C(10)	C(15)	1.40 (1)
Rh(1)	C(55)	1.78 (1)	O(2)	C(8)	1.44 (1)	C(19)	C(20)	1.39 (1)
Rh(1)	O(1)	2.319 (7)	O(3)	C(6)	1.34 (1)	C(19)	C(24)	1.40 (2)
Rh(1)	O(18)	2.611 (7)	O(3)	C(9)	1.41 (2)	C(28)	C(29)	1.41 (1)
P(1)	C(1)	1.81 (1)	O(19)	C(55)	1.14 (1)	C(28)	C(33)	1.40 (1)
P(1)	C(10)	1.81 (1)	C(1)	C(2)	1.39 (1)	C(37)	C(38)	1.39 (1)
P(1)	C(19)	1.829 (9)	C(1)	C(6)	1.40 (1)	C(37)	C(42)	1.40 (1)
P(2)	C(28)	1.826 (9)	C(2)	C(3)	1.40 (2)	C(46)	C(47)	1.39 (2)
P(2)	C(37)	1.83 (1)	C(3)	C(4)	1.37 (1)	C(46)	C(51)	1.37 (1)
P(2)	C(46)	1.83 (1)	C(4)	C(5)	1.40 (1)			
O(1)	C(2)	1.36 (1)	C(5)	C(6)	1.37 (2)			

Bond Angles

atom 1	atom 2	atom 3	angle	atom 1	atom 2	atom 3	angle	atom 1	atom 2	atom 3	angle
P(1)	Rh(1)	P(2)	175.0 (1)	Rh(1)	O(1)	C(2)	121.2 (5)	O(3)	C(6)	C(5)	123.3 (9)
P(1)	Rh(1)	O(1)	78.1 (2)	Rh(1)	O(1)	C(7)	118.9 (6)	C(1)	C(6)	C(5)	121.5 (9)
P(1)	Rh(1)	C(55)	91.3 (3)	C(2)	O(1)	C(7)	118.4 (9)	P(1)	C(10)	C(11)	116.9 (7)
P(2)	Rh(1)	O(1)	103.2 (2)	C(4)	O(2)	C(8)	117.5 (9)	P(1)	C(10)	C(15)	127.8 (7)
P(2)	Rh(1)	C(55)	89.3 (3)	C(6)	O(3)	C(9)	119 (1)	C(11)	C(10)	C(15)	115.0 (9)
O(1)	Rh(1)	C(55)	150.2 (4)	C(15)	O(6)	C(18)	120 (1)	P(1)	C(19)	C(20)	126.7 (8)
Rh(1)	P(1)	C(1)	104.3 (3)	P(1)	C(1)	C(2)	119.3 (8)	P(1)	C(19)	C(24)	115.6 (6)
Rh(1)	P(1)	C(10)	117.5 (3)	P(1)	C(1)	C(6)	122.8 (7)	C(20)	C(19)	C(24)	117.5 (8)
Rh(1)	P(1)	C(19)	110.1 (4)	C(2)	C(1)	C(6)	118 (1)	P(2)	C(28)	C(29)	126.7 (7)
C(1)	P(1)	C(10)	104.8 (5)	O(1)	C(2)	C(1)	117.0 (9)	P(2)	C(28)	C(33)	117.0 (7)
C(1)	P(1)	C(19)	111.1 (4)	O(1)	C(2)	C(3)	121.8 (8)	C(29)	C(28)	C(33)	115.5 (8)
C(1)	P(1)	C(19)	108.8 (4)	C(1)	C(2)	C(3)	121.2 (9)	P(2)	C(37)	C(38)	130.0 (7)
Rh(1)	P(2)	C(28)	112.5 (4)	C(2)	C(3)	C(4)	119.2 (9)	P(2)	C(37)	C(42)	114.1 (7)
Rh(1)	P(2)	C(37)	113.9 (3)	O(2)	C(4)	C(3)	124.3 (9)	C(38)	C(37)	C(42)	116 (1)
Rh(1)	P(2)	C(46)	110.0 (3)	O(2)	C(4)	C(5)	115.0 (9)	P(2)	C(46)	C(47)	120.9 (6)
C(28)	P(2)	C(37)	109.5 (4)	C(3)	C(4)	C(5)	121 (1)	P(2)	C(46)	C(51)	120.2 (8)
C(28)	P(2)	C(46)	108.9 (4)	C(4)	C(5)	C(6)	120 (1)	C(47)	C(46)	C(51)	118.7 (9)
C(37)	P(2)	C(46)	101.4 (5)	O(3)	C(6)	C(1)	115 (1)	Rh(1)	C(55)	O(19)	176 (1)

reported for several other mononuclear Rh(II) complexes.[10a]

Crystal Structure of $[Rh(\eta^3\text{-TMPP})_2][BF_4]_2$ (1). The molecular cation shown in Figure 1, consists of two phosphine ligands bonded to the Rh atom in a face-capping tridentate mode through the oxygen atoms of two pendant methoxy groups and the phosphorus atom. This bonding arrangement of TMPP is identical to that observed in the molybdenum tricarbonyl complex $Mo(CO)_3(\eta^3\text{-TMPP})$.[29] The geometry about the Rh center is a distorted

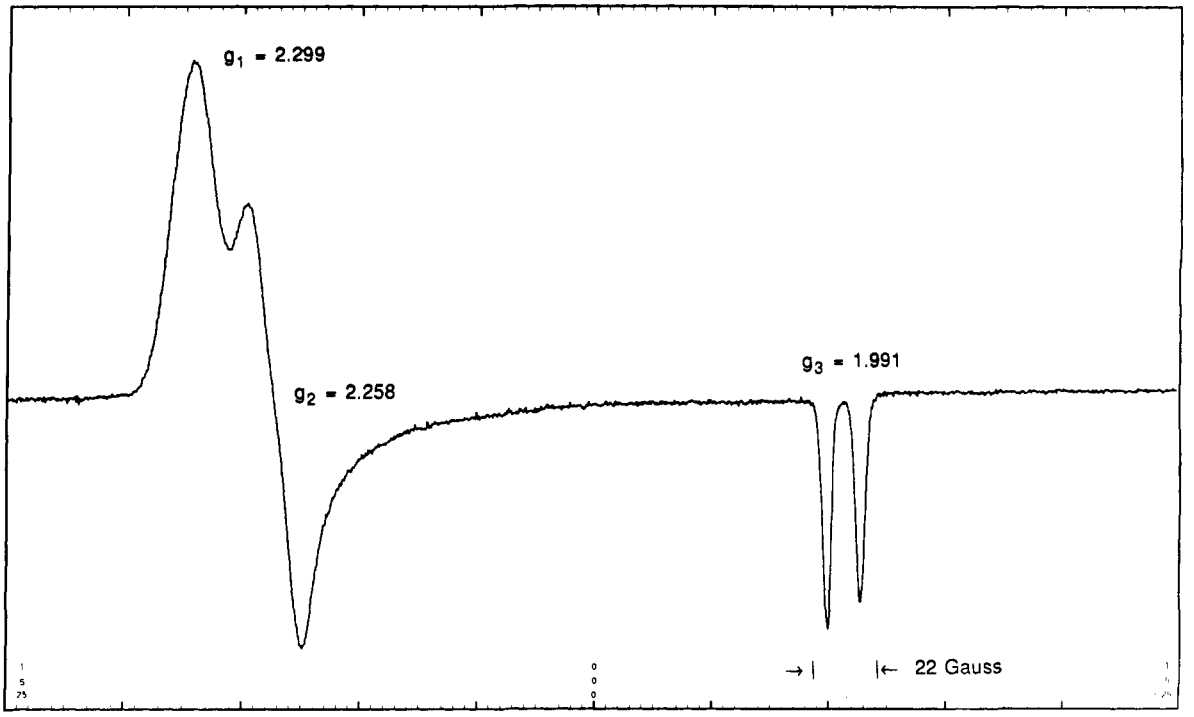

Figure 5. EPR spectrum of $[Rh(\eta^3\text{-TMPP})_2][BF_4]_2$ (**1**) in a CH_2Cl_2/Me-THF glass at 77 K.

octahedron, with the Rh atom residing on a 2-fold axis that bisects the P–Rh–P′ angle. Perhaps the most striking feature of the structure is the fact that the phosphines lie cis to each other rather than in the expected trans arrangement based on steric arguments. The consequences of steric repulsion brought about by the cis geometry in the structure of **1** are evident in the P(1)–Rh–P(1)′ bond angle of 105.2 (1)°. Indeed Rh(II) complexes with the formula RhX_2L_2 where L is a bulky tertiary phosphine have been postulated to contain trans phosphines, although this is difficult to prove without the availability of structural information afforded by NMR spectral data. It is conceivable that the cis complex is a kinetic product, but we have been unsuccessful in effecting an isomerization to a more sterically favorable, trans geometry at higher temperatures. It is interesting in the context of this discussion to note that Rauchfuss et al. also observed a cis arrangement of $PPh_2(o\text{-}MeOC_6H_4)$ groups for the complex $RuCl_2(PR_3)_2$, in which the ether phosphine also participated in a chelating interaction with the metal.[6d] Furthermore Shaw noted similar cis isomers in the reaction of $PPh_2(C_6H_4OH)$ with Pd and Pt chlorides.[30] In the case of **1**, the chelation results in the formation of a five-membered metallacyclic ring, the geometric requirements of which distort the molecule as evidenced by the strained P(1)–Rh(1)–O(6) bond angles of 77.9 (2)° and 80.5 (1)°. This distortion is of the same magnitude as that observed for other complexes containing similar chelate rings, such as $RhCl_3(AsR_3)_2$,[5] $RuCl_2(PR_3)_2$,[6d] and $Mo(CO)_3(\eta^3\text{-TMPP})$.[29]

The distances within the immediate coordination sphere of Rh are worth commenting upon as they show some unusual features. The Rh(1)–P bond distance of 2.216 (2) Å is significantly shorter than the corresponding distances found in most Rh(I) and Rh(III) phosphine complexes; these are generally on the order of 2.28 to 2.37 Å.[31] As for the Rh–P bond distances in other mononuclear Rh(II) compounds, the two structurally characterized compounds of which we are aware, *trans*-$RhCl_2(PPh_3)_2$ and $RhCl(PPh_3)_2Cl$(s-bqdi) (s-bqdi = semi-*o*-benzoquinonediimine), exhibit slightly longer Rh–P bonds, 2.323 (2), 2.277, and 2.330 Å, respectively.[26,32] In $RhCl_2(PPh_3)_2$, the phosphines exert a significant trans effect on one another, and so one would expect a lengthening of the Rh–P bonds. In contrast, complex **1** contains ether donors in positions opposite to the phosphorus donors; these would be expected to exhibit little if any trans effect. Indeed the Rh–O bond distances in **1** are quite long as compared to those of metal alkoxides or other anionic oxygen donor ligands and are indicative of the weak nature of the Rh–ether bond.[33] Rauchfuss arrived at a similar conclusion upon observing that $RuCl_2(PR_3)_2$, with phosphorus atoms trans to methoxy groups, exhibits Ru–P bond distances that are much shorter than in other Ru(II) phosphine complexes.[6d]

Of further importance in the solid-state structure of $[Rh(\eta^3\text{-TMPP})_2]^{2+}$ is the presence of two chemically distinct metal–ether interactions. The oxygen atoms trans to phosphorus are bonded at a distance of 2.201 (6) Å, whereas the mutually trans oxygen atoms exhibit Rh–O distances of 2.398 (1) Å. The axial elongation is undoubtedly the result of a Jahn–Teller distortion and constitutes the first structural evidence for this effect in d^7 Rh(II) chemistry. Interestingly, although the axial ether groups are located at long distances, they afford protection from attack by donor solvents such as CH_3CN or oxidizing solvents such as CH_2Cl_2.

Redox Properties of $[Rh(\eta^3\text{-TMPP})_2][BF_4]_2$ (1): Oxidation to $[Rh(\eta^3\text{-TMPP})_2][BF_4]_3$ (2). A cyclic voltammogram of $[Rh(\eta^3\text{-TMPP})_2][BF_4]_2$ (**1**) (shown in Figure 6) exhibits two accessible redox couples, one reversible oxidation at +0.46 V and a quasi-reversible reduction at −0.65 V (vs Ag/AgCl). Accordingly, we expected that **1** would undergo chemical redox reactions to form Rh(I) and Rh(III) compounds with minimal structural rearrangement. Oxidation of **1** with either $[NO][BF_4]$ or $[Cp_2Fe][BF_4]$ in CH_3CN or CH_2Cl_2 results in the formation of a deep red solution of $[Rh(\eta^3\text{-TMPP})_2][BF_4]_3$ (**2**). The product was isolated as an oily solid by addition of Et_2O or evaporation of the solvent. Complex **2** is both air-sensitive and thermally unstable. The latter point is illustrated by the fact that solutions of **2** readily decompose at ambient temperatures (vide infra). To circumvent this problem, the synthesis of **2** was carried out at −40

(29) Dunbar, K. R.; Haefner, S. C.; Burzynski, D. J. *Organometallics* **1990**, *9*, 1347.
(30) Empsall, H. D.; Shaw, B. L.; Turtle, B. L. *J. Chem. Soc., Dalton Trans.* **1976**, 1500.
(31) Corbridge, D. E. C. *The Structural Chemistry of Phosphorus*; Elsevier: Amsterdam, 1974; Chapter 11.
(32) Peng, S. M.; Peters, K.; Peters, E. M.; Simon, A. *Inorg. Chim. Acta* **1985**, *101*, L35.
(33) (a) Chebi, D. E.; Fanwick, P. E.; Rothwell, I. P. *Polyhedron* **1990**, *9*, 969. (b) Mehrotra, R. C.; Agarwal, S. K.; Singh, Y. P. *Coord. Chem. Rev.* **1985**, *68*, 101. (c) Boyar, E. B.; Robinson, S. D. *Coord. Chem. Rev.* **1983**, *50*, 109. (d) Graham, D. E.; Lamprecht, G. J.; Potgieter, I. M.; Roudi, A.; Leipoldi, J. G. *Trans. Met. Chem.* **1991**, 193.

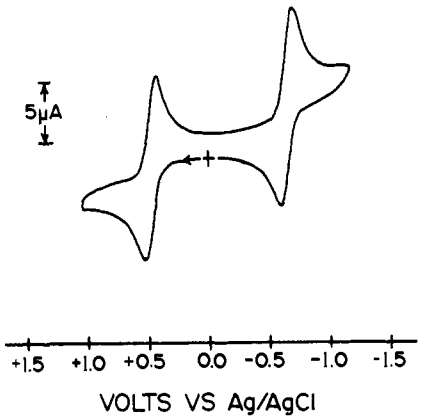

Figure 6. Cyclic voltammogram of $[Rh(\eta^3\text{-TMPP})_2][BF_4]_2$ (**1**) in 0.1 M $[(n\text{-Bu})_4N][BF_4]$–CH_2Cl_2 solution at a scan rate of 200 mV/s using a Pt working electrode and a Ag counter electrode.

°C. The cyclic voltammogram of **2** is identical to that of **1** except that the two redox couples correspond to one-electron reductions to form Rh(II) and Rh(I) species (Figure 7a). Schröder[12b] and Cooper[12a,c] independently reported analogous electrochemical behavior for the homoleptic Rh(III) thioether complexes $[Rh(9S3)_2]^{3+}$, $[Rh(10S3)_2]^{3+}$, and $[Rh(12S3)_2]^{3+}$, for which both the Rh(II) and Rh(I) oxidation states are accessible.

Infrared spectral measurements of **2** show a typical pattern for coordinated TMPP in addition to a strong broad band at 1050 cm^{-1} corresponding to the BF_4^- counterion. The ^1H NMR spectrum of **2** in CD_2Cl_2 contains nine resonances between δ 2.93 and δ 4.69 corresponding to the methoxy substituents of two magnetically equivalent TMPP ligands. Further downfield there are six poorly resolved doublets of doublets of equal intensity in the meta region of the phenyl rings. The ABX pattern of the resonance corresponds to coupling of one aromatic proton to the other ring proton and to the phosphorus nucleus. The ^{31}P NMR spectrum in CD_2Cl_2 shows a doublet centered at δ 37.4 ppm (J_{Rh-P} = 107 Hz), further indicating that the two TMPP ligands are equivalent. Therefore, it appears that the ABX pattern of the meta protons arises from coupling of proximal and distal protons on the individual chelate rings, with further coupling to the phosphorus. Although only two rings participate in the chelation to the metal, it is apparent that the meta protons on the third noninteracting ring are also magnetically inequivalent as these protons exhibit an ABX pattern. This suggests that the noninteracting ring is sterically locked into an asymmetric environment and is unable to rotate freely about the P–C bond, thereby rendering the protons inequivalent.

Crystal Structure of $[Rh(\eta^3\text{-TMPP})_2][BF_4][PF_6]_2$ (2). A preliminary X-ray crystal study of **2** shows that the Rh atom lies on a 2-fold axis that bisects the *cis*-phosphine ligands as in the structure of the parent complex $[Rh(\eta^3\text{-TMPP})_2]^{2+}$ (**1**). As established by solution ^1H NMR studies, each TMPP binds to the metal in the familiar capping tridentate fashion observed in the structure of **1** and in the molecule $Mo(CO)_3(\eta^3\text{-TMPP})$.[29] Difficulties encountered while modeling a disorder of the $[BF_4]^-$ anion precluded a satisfactory refinement of the structure in this region. Details of the structure in its present form have been deposited in the supplementary material section.

Decomposition of $[Rh(\eta^3\text{-TMPP})_2][BF_4]_3$ (2). As mentioned earlier, solutions of $[Rh(TMPP)_2][BF_4]_3$ are thermally unstable with respect to loss of a methyl group to form $[Rh(\eta^3\text{-TMPP})(P\{C_6H_2(OMe)_3\}_2\{C_6H_2(OMe)_2O\})][BF_4]_2$ (**5**). At room temperature, NMR samples of **2** in CD_2Cl_2 show evidence of de-

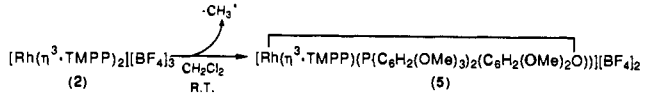

methylation within minutes, but upon cooling to −20 °C, the process is slowed. Demethylation occurs regardless of solvent choice, but the reaction is faster in acetone and acetonitrile than

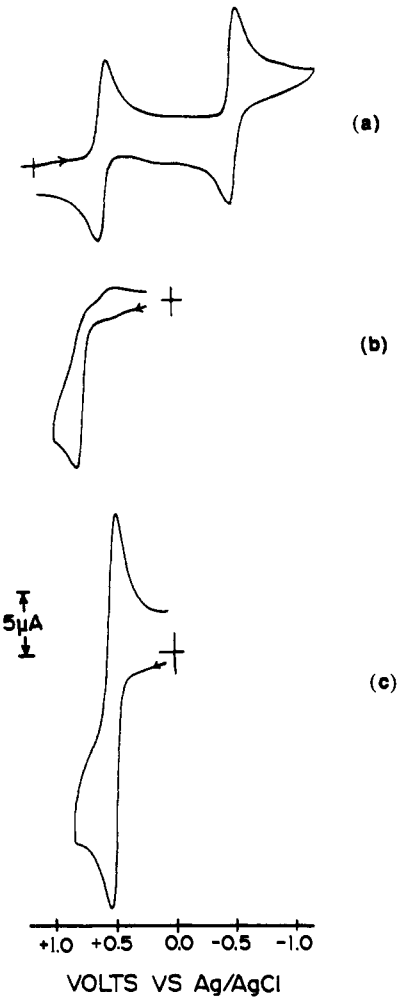

Figure 7. Cyclic voltammograms in 0.1 M $[(n\text{-Bu})_4N][BF_4]$–CH_2Cl_2 at a scan rate of 200 mV/s using a Pt working electrode and a Ag counter electrode for (a) $[Rh(\eta^3\text{-TMPP})_2][BF_4]_3$ (**2**), (b) $[Rh(TMPP)_2(CO)_2][BF_4]$ (**3**), and (c) $[Rh(\eta^2\text{-TMPP})(TMPP)(CO)][BF_4]$ (**4**).

in methylene chloride. The process is quite facile, as evidenced by the fact that even solid samples of **2** slowly convert to **5** over a period of weeks at room temperature. If one heats the sample to 50 °C, nearly quantitative conversion of **2** to **5** occurs within 36 h in the solid state.

Compound **5** was prepared in bulk by stirring solutions of $Rh(\eta^3\text{-TMPP})_2[BF_4]_3$ at room temperature in acetone for 12 h; during this time the solution color changed from deep red to orange. The product was isolated as a pale orange solid by addition of diethyl ether, and while its infrared spectrum is nearly indistinguishable from that of $[Rh(\eta^3\text{-TMPP})_2][BF_4]_3$, the ^1H NMR spectrum reveals magnetic inequivalence of the two phosphine ligands. The spectrum, shown in Figure 8, displays nine distinct resonances between δ 5.84 and 6.96 with an ABX coupling pattern and a set of three overlapping signals centered about 5.60 ppm. Upfield resonances between δ 4.51 and δ 2.94 correspond to the *o*- and *p*-methoxy substituents on the phenyl rings and number 17 by integration, as compared to 18 in $[Rh(\eta^3\text{-TMPP})_2]^{3+}$ complex, thereby confirming the loss of a methyl group from one of the methoxy substituents. The reaction was monitored by ^1H NMR both in acetone-d_6 and in CD_2Cl_2; these studies revealed the onset of new resonances for **5**, but none that could be assigned to the protons of a methylated byproduct. This observation is consistent with the formation of a volatile species which we believe to be CFH_3 resulting from attack of BF_4^- on the complex.

^{31}P NMR spectral measurements of **5** (Figure 8) reveal two resonances with an ABX splitting pattern at δ 37.9 for P_A ($^1J_{Rh-P}$ = 138.9 Hz, $^2J_{P-P}$ = 13.73 Hz) and δ 31.5 for P_B ($^1J_{Rh-P}$ = 140.4 Hz, $^2J_{P-P}$ = 13.73 Hz). From these data it is possible to assign the coordination geometry about the metal center.[34] The small

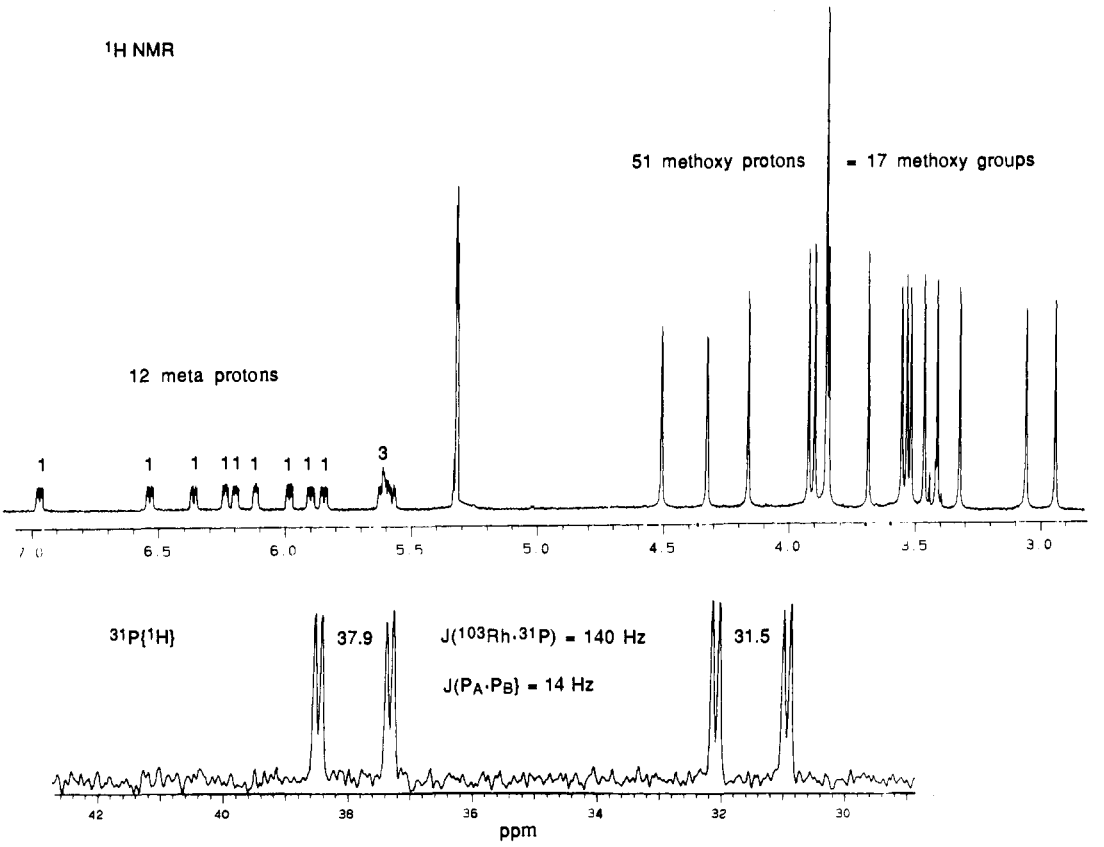

Figure 8. ^1H and $^{31}P\{^1H\}$ NMR spectra of $[Rh(\eta^3\text{-TMPP})(\eta^3\text{-TMPP-}O)][BF_4]_2$ (**5**) in CD_2Cl_2.

magnitude of the P–P coupling is indicative of a cis disposition of phosphines,[35] and the similarity in the two Rh–P coupling constants suggests that the phenoxide interaction is cis to both P atoms. Presence of a Rh–phenoxide bond in a trans disposition to one of the P nuclei would be expected to result in a larger difference in the Rh–P coupling constants. The structure of **5** is rationalized by considering that a methoxy interaction with a metal center weakens the $O\text{–}CH_3$ bond thus rendering the carbon susceptible to nucleophilic attack. It follows that the stronger the metal–oxygen interaction, the more electrophilic the methyl group becomes. Methoxy groups exert a weaker trans influence than the phosphorus atoms, resulting in stronger M–O interactions for the mutually trans methoxy groups than for those trans to the phosphines. It is worth noting that dealkylation of ether groups in methoxyphosphines has been previously observed, including a dirhodium carboxylate complex prepared in our laboratories, but, in contrast to the present study, these were found to occur under more forcing conditions and in the presence of much stronger nucleophiles.[36,37] The instability of $[Rh(\eta^3\text{-TMPP})_2][BF_4]_3$ (**2**) may, in part, be explained by the relatively hard nature of Rh^{3+} compared to that of other platinum group metals in the 1+ and 2+ oxidation states. Furthermore, Shaw reported that the ease of dealkylation increased as the steric bulk of the ancillary substituents on the phosphine was increased.[37b] It is reasonable to assume that the considerable bulk of the methoxy-substituted phenyl rings of TMPP contributes to facile demethylation of $[Rh(\eta^3\text{-TMPP})_2][BF_4]_3$ (**2**).

Electrochemical measurements performed on CH_2Cl_2 solutions of **5** show that the molecule undergoes an irreversible oxidation at $E_{p,a} = +1.55$ V vs Ag/AgCl that most likely corresponds to a ligand process based on the fact that free TMPP undergoes an oxidation near this potential. In addition, **5** exhibits an irreversible reduction at $E_{p,c} = -0.80$ V vs Ag/AgCl with a coupled chemical oxidation wave at −0.02 V vs Ag/AgCl. Chemical reduction with cobaltocene yields a deep red solution which exhibits a broad ^1H NMR signal characteristic of a paramagnetic compound. The latter species resembles the product obtained by the direct reaction of $[Rh(\eta^3\text{-TMPP})_2][BF_4]_2$ with additional TMPP; we believe that the two products obtained by both routes are the Rh(II) analogue of **5**, i.e., a Rh(II) phosphino–phenoxide complex.

Reactivity of $[Rh(\eta^3\text{-TMPP})_2][BF_4]_2$ (1) with Carbon Monoxide. Solutions of **1** in CH_2Cl_2 react smoothly with CO at ambient temperatures and pressures. Within 15–20 min, the initial deep purple color of **1** converts to a red-orange hue with concomitant growth of a band at $\nu(CO) = 2011$ cm^{-1}. Reactions of **1** with 1:1 mixtures of ^{12}CO and ^{13}CO gave a three band intensity pattern in the $\nu(CO)$ region, leading to the assignment of the 2011-cm^{-1} band to a dicarbonyl species. Subsequent purging with Ar or N_2 produces a new species which exhibits a lower energy CO stretch at 1970 cm^{-1}. IR monitoring studies carried out during the period of inert gas purging revealed a direct correlation between the disappearance of the species at 2011 cm^{-1} and the appearance of 1970 cm^{-1}, without the observation of other CO-containing intermediates. With longer purging times, both bands gradually decrease in intensity and finally disappear; at the same time the solution color converts from red-orange to purple. The purple product, obtained as a residue, was identified as the parent Rh(II) complex (**1**) by cyclic voltammetry, electronic spectroscopy, and EPR spectroscopy. Intrigued by the indication that we were observing reversible binding of CO to a radical d^7 metal complex, we undertook a variety of experiments to elucidate the mechanism.

(34) Meek, D. W.; Mazanec, T. J. *Acc. Chem. Res.* **1981**, *14*, 226.
(35) (a) Pregosin, P. S. *Phosphorus-31 NMR Spectroscopy in Stereochemical Analysis*; Verkade, J. G., Quin, L. D., Ed.; VCH: 1987. (b) Pregosin, P. S.; Venanzi, L. M. *Chem. Br.* **1978**, *14*, 276.
(36) (a) Chen, S. J.; Dunbar, K. R. *Inorg. Chem.* **1991**, *30*, 2018. (b) Chen, S. J.; Dunbar, K. R. *Inorg. Chem.* **1990**, *29*, 588.
(37) (a) Kurosawa, H.; Tsuboi, A.; Kawasaki, Y.; Wada, M. *Bull. Chem. Soc. Jpn.* **1987**, *60*, 3563. (b) Empsall, H. D.; Heys, P. N.; McDonald, W. S.; Norton, M. C.; Shaw, B. L. *J. Chem. Soc., Dalton Trans.* **1978**, 1119. (c) Empsall, H. D.; Heys, P. N.; Shaw, B. L. *J. Chem. Soc., Dalton Trans.* **1978**, 257. (d) Empsall, H. D.; Hyde, E. M.; Shaw, B. L. *J. Chem. Soc., Dalton Trans.* **1975**, 1690. (e) Jones, C. E.; Shaw, B. L.; Turtle, B. L. *J. Chem. Soc., Dalton Trans.* **1974**, 992. (f) Empsall, H. D.; Hyde, E. M.; Jones, C. E.; Shaw, B. L. *J. Chem. Soc., Dalton Trans.* **1974**, 1980.
(38) (a) El-Amouri, H.; Baltsoun, A. A.; Osborn, J. A. *Polyhedron* **1988**, *7*, 2035. (b) Volger, H. C.; Vrieze, K.; Praat, A. P. *J. Organomet. Chem.* **1968**, *14*, 429.

NMR Studies. NMR spectroscopy of CO-saturated CD_2Cl_2 solutions of **1** revealed that the paramagnetic starting material reacts rapidly to form two diamagnetic species at the same rate. Upon workup with Et_2O, bulk reactions carried out in CH_2Cl_2 produce a red solid and a yellow filtrate. The red solid was identified as $[Rh(\eta^3\text{-TMPP})_2][BF_4]_3$ (**2**) by ^1H and ^{31}P NMR spectroscopy (vide supra). Concentration of the yellow solution produced a crop of air-stable yellow microcrystals displaying an infrared band at $\nu(CO) = 1970\ cm^{-1}$. The ^1H NMR spectrum of **4** in CD_2Cl_2 contains three resonances: a virtual triplet at δ 6.04 ($^4J_{P-H} = 2.1$ Hz) and singlets at δ 3.80 and δ 3.48 that correspond to the meta protons of the phenyl rings, the *p*-methoxy protons, and the *o*-methoxy protons, respectively. A companion ^{31}P NMR study confirmed that the phosphorus nuclei are equivalent, with a doublet appearing at δ −11.1 ppm ($J_{Rh-P} = 128$ Hz). In light of the solid-state structure (vide infra), the ^1H NMR can be interpreted to mean that a low-energy fluxional process occurs in solution to exchange all *o*-methoxy groups. The exchange mechanism is envisioned to occur through association of a free methoxy group, leading to formation of a five-coordinate trigonal-bipyramidal structure, followed by labilization of a methoxy interaction as shown in the schematic below.[37] Upon methoxy

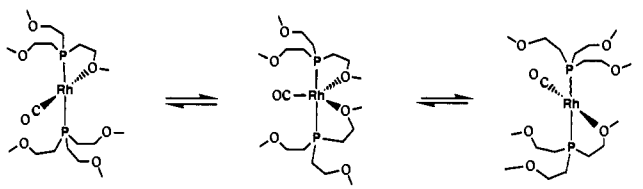

group dissociation, the phenyl ring is free to rotate about the P–C bond thereby bringing a second *o*-methoxy group into a proximal position to the metal. Rotation about the Rh–P bond eventually allows all *o*-methoxy groups on the phosphines to interact with the metal center, thus rendering the PR_3 ligands equivalent on the NMR time scale. Variable-temperature ^1H and ^{31}P NMR experiments reveal that this process continues below −90 °C, thereby attesting to the unusually high lability of the ether interactions in Rh–TMPP complexes. Similar behavior has been reported for other ether–phosphine complexes of both early and late transition metals, but, unlike the present case, low-temperature limiting spectra were observed for these fluxional complexes.[8,29]

The ease of Rh–O bond dissociation in these complexes is further evidenced by the reaction of $[Rh(\eta^2\text{-TMPP})(TMPP)CO]^+$ with another equivalent of CO. Upon exposure to an atmosphere of CO, a pale yellow solution of $[Rh(\eta^2\text{-TMPP})(TMPP)CO]^+$ converts to an intense yellow color, signifying the formation of the trans dicarbonyl species $[Rh(TMPP)_2(CO)_2]^+$. This reaction is entirely reversible with loss of carbonyl occurring after a brief period of purging with Ar or N_2. The reversible addition of CO was followed by ^1H, ^{31}P NMR, cyclic voltammetry, and electronic spectroscopy. $^{31}P\{^1H\}$ NMR measurements reveal that the ^{31}P resonance undergoes a shift from δ −11.1 ($J_{Rh-P} = 128$ Hz) ppm for **4** to δ −23.8 (d, $J_{Rh-P} = 116$ Hz) for **3** upon addition of the second carbonyl ligand. The ^1H NMR spectrum of **3** in CD_2Cl_2 shows magnetically equivalent TMPP ligands with a triplet appearing at δ 6.02 ($J_{P-H} = 2.1$ Hz) due to the meta protons and two singlets at δ 3.41 and 3.79 which integrate in the correct ratio for *o*- and *p*-methoxy groups. The symmetrical nature of the resonances indicates that rotation about the Rh–P bond is not sterically hindered by the presence of the two carbonyl ligands.

Electrochemistry of $[Rh(\eta^2\text{-TMPP})(TMPP)CO][BF_4]$ (4) and $[Rh(TMPP)_2(CO)_2][BF_4]$ (3). The cyclic voltammogram of $[Rh(\eta^2\text{-TMPP})(TMPP)(CO)]^+$ (**4**) shows a quasi-reversible oxidation at $E_{1/2(ox)} = +0.50$ V (Figure 7c). Not surprisingly, this oxidation process is less accessible than the Rh(II)/Rh(I) couple of the parent complex, $[Rh(\eta^3\text{-TMPP})_2][BF_4]_2$ (**1**).[39] The addition of a second CO ligand to give the dicarbonyl $[Rh(TMPP)_2(CO)_2]^+$ results in a large positive shift in the Rh(I)/Rh(II) couple to +0.80 V (Figure 7b). The ramifications of this shift on the overall reaction pathway are detailed in the Discussion section.

Crystal Structures of $[Rh(TMPP)_2(CO)_n][BF_4]$ ($n = 1, 2$). (i) **$[Rh(\eta^2\text{-TMPP})(TMPP)CO][BF_4]$ (4).** The solid-state structure of **4**, shown in Figure 2, consists of a $[Rh(\eta^2\text{-TMPP})(TMPP)CO]^+$ cation and a BF_4^- anion in the asymmetric unit. The geometry about the Rh center is that of a highly distorted square-planar arrangement of ligands with trans phosphine ligands and a CO ligand that is approximately trans to an oxygen atom from an interacting *o*-methoxy group (O(1)–Rh(1)–C(1) = 150.2 (4)°). To effect this bonding, a highly strained five-membered chelate ring is formed: M–P–C–C–O (P(1)–Rh(1)–O(1) = 78.1 (2)°). The presence of this rather acute angle results in a gross distortion of the structure from an ideal square-planar arrangement. Related molecules with this ligand and other ether phosphines show similar structural features.[6d,30]

The distance of 2.319 (7) Å for Rh(1)–O(1) in the present case is intermediate between the values for the axial and equatorial Rh–O distances found in $[Rh(\eta^3\text{-TMPP})_2][BF_4]_2$ (**1**). The observed high lability of the ether group in solution reflects the weakness of the bond. Of further interest in the crystal structure of **4** is the presence of a second methoxy group from the monodentate phosphine ligand at a distance of 2.611 (7) Å, a value that is outside the sum of the covalent bonding radii for Rh and O. This oxygen atom is situated in such a position so as to be prepared to occupy an equatorial site of a trigonal bipyramidal structure as the Pluto drawing in Figure 3 emphasizes. In fact we rationalize that, in solution, the methoxy group readily coordinates to the metal to form such an intermediate in order to exchange all six *o*-methoxy groups in a fluxional process.

(ii) **$[Rh(TMPP)_2(CO)_2][BF_4]$ (3).** Compound **3** crystallizes as a symmetrical molecule ligated by two phosphines and two carbonyl groups in a square-planar geometry. As was observed in the structure of **4**, the two TMPP ligands are trans to each other, but in this case each TMPP is bound through only the phosphorus atom (Figure 4). Unlike for the monocarbonyl compound, the closest approach of *o*-methoxy groups is well outside the coordination sphere of rhodium, and there are no major structural distortions as evidenced by the nearly ideal angles P(1)–Rh(1)–P(2) = 178.46 (6) Å and C(55)–Rh(1)–C(56) = 179.0 (3) Å. The second CO ties up the fourth coordination site thus eliminating the need for additional donation from an ether oxygen atom. Both the Rh–P and Rh–C bond distances fall well within the range of values expected for Rh(I) complexes and are themselves quite unremarkable.

Discussion

This paper addresses the synthesis, solution properties, redox chemistry, solid-state structure, and CO chemistry of a remarkable rhodium(II) phosphine complex. These findings are of considerable interest in the general context of small molecule binding to paramagnetic metal centers, which has been well investigated in the case of Co(II), but for which parallel studies are essentially nonexistent for Rh(II). The reason for this is undoubtedly the paucity of stable Rh(II) mononuclear species that have been established as authentic metal-based radicals. The uncertainty as to the location of the unpaired electron is especially high in the reported Rh(II) compounds with noninnocent sulfur- and nitrogen-based ligands.[10c,12e,32] As far as we are aware, $[Rh(\eta^3\text{-TMPP})_2]^{2+}$ represents the only case of a structurally characterized six-coordinate mononuclear Rh(II) complex; moreover the comprehensive study of its solution reactivity with CO constiutes the first such investigation for a paramagnetic d^7 rhodium complex. The stability of the (formally) 19e$^-$ species is attributed to the presence of four interacting ether groups which serve to stabilize the complex both electronically and sterically. Without the "built-in" coordinative saturation afforded by the tethered "solvent" molecules, one would expect the molecule to undergo the usual disproportionation or dimerization reactions commonly observed in divalent Rh chemistry. The ready availability of the dangling ether groups allows for reversibility of substitution re-

(39) Dunbar, K. R.; Walton, R. A. *Inorg. Chim. Acta* **1984**, *87*, 185.

Scheme I. Proposed Pathway for the Reversible Reaction between $[Rh(\eta^3\text{-}TMPP)_2]^{2+}$ (**1**) and CO

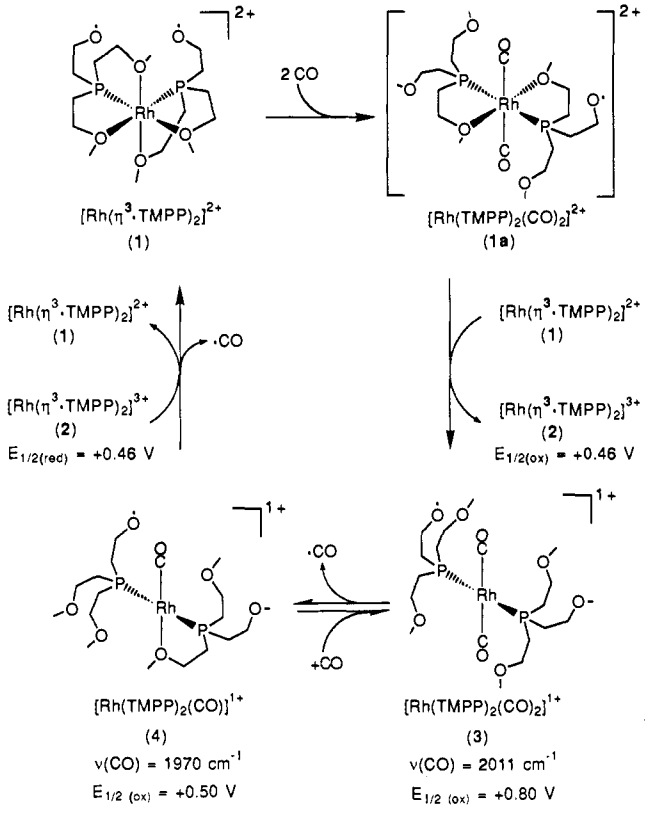

actions, a situation that is generally not possible with complexes that undergo dissociative loss of a ligand such as a phosphine.

The reversible CO chemistry of $[Rh(\eta^3\text{-}TMPP)_2][BF_4]_2$ at ambient temperature and pressure proceeds through a series of reactions which involve the formation of Rh(III) and Rh(I) complexes. The interrelationships of the five compounds involved in the cyclic reaction are depicted in Scheme I. These conclusions were arrived at by establishing independent synthetic routes to intermediates **2**–**4** and subsequently investigating their spontaneous redox behavior and reactivity with CO. Scheme II outlines rational pathways to the key compounds **2**–**4** as well as their interconversions and reactions with CO.

There are several key features of the chemistry in Scheme I which must be emphasized in any discussion of this work. The initial attack of CO on the Rh(II) complex **1** is slow; therefore, unreacted starting material is in large excess during the early stages of the reaction. While we never definitively characterized the adducts $Rh^{II}(CO)_x$ (x = 1, 2) (although we attempted to do so by in situ infrared and EPR studies), their existence is predicated on the basis of the available redox properites of the other intermediates along the reaction pathway. The fact that **1a** is too short-lived to be observed by ordinary spectroscopic methods is explained by the very fast electron-transfer reaction that takes place between **1** and the strong oxidant **1a** to produce a 50:50 mixture of $[Rh(\eta^3\text{-}TMPP)_2][BF_4]_3$ (**2**) and $[Rh(TMPP)_2(CO)_2][BF_4]$ (**3**). Indeed, experiments carried out in NMR tubes under a ^{12}CO atmosphere showed that two diamagnetic products were being produced at the same rate and that they were stable with respect to further reaction—provided the CO atmosphere was maintained. A parallel study using a 50:50 mixture of $^{12}CO/^{13}CO$ provided solution evidence for the assignment of **3** as a dicarbonyl species. A subsequent X-ray structural study verified this formulation. Under conditions of pumping or purging with an inert gas, **3** loses a CO ligand to form **4**, a molecule that is unstable with respect to oxidation by the Rh(III) complex **2** to yield Rh(II) and presumably $Rh^{II}(CO)^{\bullet}$ which readily gives up a CO to regenerate **1**. The proposed spontaneous redox reaction between **2** and **4** was confirmed by a deliberate 1:1 reaction of the pure compounds as shown in the equation below. Note that

Scheme II. High Yield Routes to Compounds **1**–**5**[a]

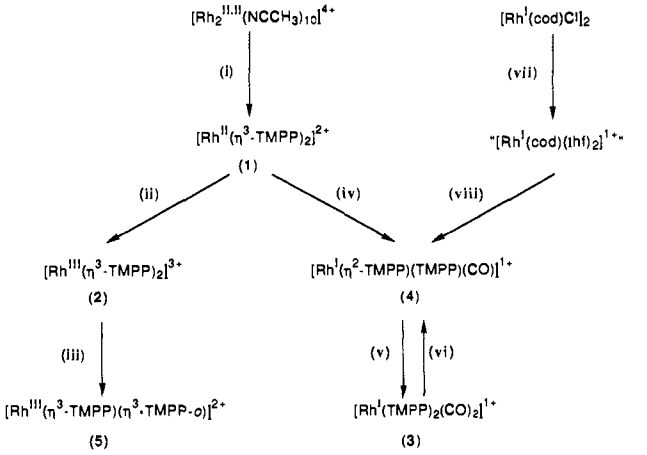

[a] (i) TMPP (4 equiv), MeCN, 0 °C; (ii) $NOBF_4$, MeCN, −40 °C or $[Cp_2Fe][BF_4]$, CH_2Cl_2, −40 °C; (iii) acetone, room temperature, 24 h; (iv) Cp_2Co (excess), CO, CH_2Cl_2; (v) CO, room temperature; (vi) Ar, room temperature; (vii) $AgBF_4$ (2 equiv), THF; (viii) CO, TMPP (2 equiv), 0 °C.

no reaction occurs between $[Rh(\eta^3\text{-}TMPP)_2][BF_4]_3$ and $[Rh(TMPP)_2(CO)_2][BF_4]$.

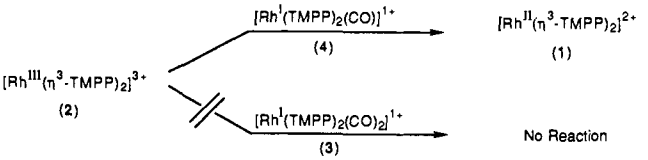

While the overall pathway described in Scheme I does not represent a simple procedure for reversible CO binding, the reaction between **3** and **4** is such a process.[40] This behavior is intriguing in the context of CO sensors, particularly if the reaction of interest exhibits the combined characteristics of (a) reversibility, (b) selectivity, (c) sensitivity, and (d) ease of detection.[41] Preliminary studies of $[Rh(\eta^2\text{-}TMPP)(TMPP)CO][BF_4]$ (**4**) indicate that the complex is unreactive to all other atmospheric gases besides CO, a result that also holds true in the solid state. Powder or Nujol mull samples of **4** were seen to uptake CO reversibly at atmospheric pressure by IR spectroscopy; immobilized forms of **4** prepared in polymer films are very reactive as well, with no evidence for decomposition even after long periods of aging. Further work on the development of these and related ether–phosphine complexes as potential sensors for CO and other small molecules is in progress.[42]

Finally, we turn to a discussion of the major influence on the observed chemistry of $[Rh(\eta^3\text{-}TMPP)_2]^{2+}$, viz the flexibility of the ligand. Unlike most other sterically hindered ligands, TMPP allows the metal complex to undergo labilization of weakly held groups and isomerization to more stable geometries. The structures of the *trans*-Rh(I) complexes **3** and **4** nicely demonstrate this point. It is precisely the lack of structural rigidity that permits complexes of ether phosphines such as TMPP to undergo reversible small molecule addition reactions. Hypothetically, an approach to stabilizing Rh(II) adducts would be to anchor the TMPP ligand at two points rather than just at the M–P bond, a situation that would prevent free rotation of the phosphine. One such reaction to effect this result is nucleophilic attack on a coordinated methoxy

(40) Examples of reversible addition of CO to mononuclear complexes: (a) Schrock, R. R.; Osborn, J. A. *J. Am. Chem. Soc.* **1971**, *23*, 2397. (b) Chatt, J.; Butler, S. A. *J. Chem. Soc., Chem. Commun.* **1967**, 501. (c) Lindner, E.; Norz, H. *Z. Naturforsch.* **1989**, *44b*, 1493. (d) Taqui Khan, M. M.; Kureshy, R. I.; Kahn, N. H. *Inorg. Chim. Acta* **1991**, *181*, 119.

(41) Mirkin, C. A.; Wrighton, M. S. *J. Am. Chem. Soc.* **1990**, *112*, 8596, and references therein.

(42) Berglund, K. A.; Dulebohn, J. I.; Dunbar, K. R.; Haefner, S. C., manuscript in preparation.

group to produce a stronger metal–phenoxide interaction. An anionic oxygen is not as susceptible to dissociation as an ether substituent, thus it is unlikely that substitution chemistry with CO would follow the same pathway as that found in this study. Support for this concept is found in the fascinating work of Wayland et al. who discovered that the rigid framework of bulky porphyrin Rh(II) complexes provided an ideal template for the coupling of CO ligands;[43] it is worthwhile to investigate rigid P–O based ligand systems to see if similar behavior will result.

Another approach to the stabilization of Rh^{II}TMPP small molecule products is to increase the size of the incoming group. To this end, we recently extended our studies of $[Rh(\eta^3\text{-TMPP})_2]^{2+}$ to include reactions with RNC (R = Me, ^{i}Pr, ^{t}Bu).[44] In the cases where R = ^{i}Pr and ^{t}Bu, we isolated and structurally characterized the paramagnetic isocyanide products of general formula $[Rh(CNR)_2(TMPP)_2][BF_4]_2$. Besides providing the very first examples of stable π-acceptors complexes of divalent rhodium, this work lends credence to our earlier prediction about the possible formation of a $Rh^{II}(CO)_2^{\bullet}$ intermediate in the carbon monoxide chemistry. The results found for the larger R group isocyanides are to be contrasted with that observed for MeNC which follows a reaction course similar to that of CO, i.e., with no detectable $Rh^{II}(CNMe)_x^{\bullet}$ adducts. From this, we conclude that while kinetic stabilization is probably an important factor in dictating the course of the reactions with π-acceptors ligands, the modulation of the electron density at the metal center (a factor that controls the accessibility of the Rh(II)/Rh(III) couple) is also a primary determinant. Further studies aimed at elucidating the fine details of these reactions are in progress. Curiously, although $[Rh(\eta^3\text{-TMPP})_2]^{2+}$ undergoes ether group dissociation and subsequent cis → trans isomerization in favor of π-acceptors such as CO and CNR (R = Me, ^{i}Pr, ^{t}Bu),[44] it is unreactive toward donors such as O_2. This is evidently a consequence of the electronic environment of the metal rather than a steric effect, since identical behavior has been noted for ether–phosphine complexes in which the ligand is not particularly bulky.[6d]

(43) (a) Wayland, B. B.; Sherry, A. E.; Coffin, V. L. *J. Chem. Soc., Chem. Commun.* **1989**, 662. (b) Wayland, B. B.; Sherry, A. E. *J. Am. Chem. Soc.* **1989**, *111*, 5010.

(44) Dunbar, K. R.; Haefner, S. C., manuscript in preparation.

Conclusion

The work described above is the first full account of the synthesis, magnetic, solid-state, and spectroscopic properties of an authentic divalent mononuclear rhodium complex. Carbon monoxide reactions of the Rh(II) bisphosphine complex show complicated but reversible behavior which involve essentially three reactions before one cycle is complete. There appears to be rich redox and small molecule binding chemistry associated with the use of the tris(2,4,6-trimethoxyphenyl)phosphine ligand, thus extensions of the present work to a variety of metals and substrates appears attractive.

Acknowledgment. We gratefully acknowledge the National Science Foundation (P.I. Grant CHE-8914915), Michigan State University (Research Initiation Grant), and the Camille and Henry Dreyfus Foundation for providing funding for this work. We also thank Dow Chemical Company and Michigan State University College of Natural Science for Research Fellowships for S.C.H., and Johnson Matthey for a generous loan of $RhCl_3 \cdot xH_2O$. We thank Dr. Colleen Partigianoni for help with the ^{13}CO studies. X-ray equipment was supported by a grant from the National Science Foundation (Grant CHE-8403823 and CHE-8908088). NMR equipment was supported by grants from the National Science Foundation (Grant CHE-88-00770) and the National Institutes of Health (Grant. No. 1-S10-RR04750-01).

Registry No. 1, 121757-68-4; **2**, 136889-87-7; **3**, 134788-86-6; **3**·CH_2Cl_2, 134788-87-7; **4**, 134821-08-2; **4**·$2C_6H_6$, 134821-09-3; **5**, 136827-10-6; TMPP, 91608-15-0; $[Rh_2(CH_3CN)_{10}][BF_4]_4$, 117686-94-9; $[Rh(cod)Cl]_2$, 12092-47-6.

Supplementary Material Available: Tables of crystallographic parameters, atomic positional and thermal parameters, full bond distances and angles, and anisotropic thermal parameters, collection procedures, and a stereoview of **2** (75 pages); a listing of observed and calculated structure factors (167 pages). Ordering information is given on any current masthead page.